NASA TN D-1360

NASA TN D-1360

28

TECHNICAL NOTE

D-1360

THE ELECTROMAGNETIC-RADIATION ENVIRONMENT OF A SATELLITE

PART I. RANGE OF THERMAL TO X-RADIATION

By S. Katzoff

Langley Research Center
Langley Station, Hampton, Va.

NATIONAL AERONAUTICS AND SPACE ADMINISTRATION
WASHINGTON
September 1962

CONTENTS

NATIONAL AERONAUTICS AND SPACE ADMINISTRATION

TECHNICAL NOTE D-1360

THE ELECTROMAGNETIC-RADIATION ENVIRONMENT OF A SATELLITE

PART I. RANGE OF THERMAL TO X-RADIATION*

By S. Katzoff

SUMMARY

This paper reviews the present literature on the short-wavelength (thermal to X-ray) electromagnetic radiation that may strike a satellite of the Earth, the Moon, Mars, or Venus. Most of the emphasis is on solar radiation and on planetary reflected radiation and thermal radiation, with some detailed discussion of the spectral composition and variability of the reflected and thermal radiation from the Earth. The lesser sky radiations such as the airglow, the zodiacal light, and starlight are also briefly discussed.

INTRODUCTION

The present paper is a review of the short-wavelength (thermal to X-ray) electromagnetic-radiation environment of a satellite of the Earth, the Moon, Mars, or Venus. Its purpose is to provide some of the environment information that might be required by the designer of a satellite or by the designer of an experiment to be carried on it. Secondary purposes are to provide a representative bibliography and to indicate where deficiencies exist in the available information. The short-wavelength radiation is mainly of interest with regard to the thermal balance of a satellite; however, the more energetic radiation is of further interest because it can cause deterioration of satellite materials and also because it can produce other photochemical or photoelectric effects that may interfere more or less directly with the scientific experiments or the instrumentation.

The material presented has been organized in terms of (1) direct solar radiation, including the farther ultraviolet and X-ray regions of the spectrum, (2) solar radiation reflected from the planet or the Moon, (3) thermal radiation emitted by the planet or the Moon. Much of the discussion of reflected and thermal radiations pertains to the Earth, for which considerable information is available. There is less detail for the reflected and thermal radiations from the Moon, Mars, and Venus.

*Part II. Radio Waves, by Jerry L. Modisette, is NASA Technical Note D-1361.

Some discussion has also been included of the lesser sky radiations in or near the visible range.

No effort has been made to discuss the computational procedures by which the planetary radiation and reflection characteristics are translated into input at the satellite. Reference 1 might be cited as a basic source not only for the methods of making such calculations but also for extensive calculated results for the neighborhood of a uniform sphere whose reflection and radiation characteristics obey Lambert's law.

SOLAR RADIATION, WAVELENGTHS LESS THAN 10μ

Main Solar Spectrum

Table I and the upper curve of figure 1 give the energy distribution in the solar spectrum between wavelengths λ of 0.2μ and 10μ, as received at the Earth outside the atmosphere. These data are from reference 2. Later reviews (for example, ref. 3) did not result in substantially different spectra. The third column of table I gives the percentage of the total energy contained in the part of the spectrum to the left of (that is, for all wavelengths less than) the indicated wavelength. It can be seen that the spectrum up to 2.6μ contains 97 percent of the total energy and the spectrum up to 4μ contains 99 percent of the total energy.

The intensities shown in the figure and table, and the integrated intensity (2.00 cal/cm^2/min = 1,400 watts/meter^2) correspond to the solar radiation at the Earth when the Earth is at its mean distance from the Sun, that is, at a distance of 1 astronomical unit. In January, when the Earth is at perihelion, the values are higher by 3.4 percent; and in July, when the Earth is at aphelion, they are lower by the same amount. The following table gives the factors by which the given intensities must be multiplied in order to give the maximum and minimum intensities in the neighborhoods of the Moon and the Planets. The factors are merely the inverse squares of the perihelion and aphelion distances, in astronomical units.

	Solar radiation intensity / Intensity at 1 A.U.			
	Moon	Earth	Venus	Mars
Maximum . . .	1.040	1.034	1.940	0.523
Minimum . . .	.962	.967	1.885	.361

The solar radiation intensity undergoes sporadic variations, particularly at times of solar activity; however, the variations are probably never significant with regard to thermal balance of satellites. A systematic variation of 2 percent between solar maximum and solar minimum is indicated by the study reported in reference 4.

The brightness of the center of the solar disk is 1.22 times the average brightness of the disk. In addition, because of the limb reddening, the center is bluer than the average. The ratio of the center brightness to the average brightness is 1.47 at $\lambda = 0.32\mu$, 1.32 at $\lambda = 0.45\mu$, 1.16 at $\lambda = 0.80\mu$, and 1.07 at $\lambda = 2.0\mu$.

Ultraviolet Spectrum

The part of the spectrum that is below 0.2μ contains only 0.01 percent of the total energy. It is of considerable interest, however, not only for its relation to solar physics, but also because of the various photochemical and photoelectric phenomena that the higher-energy photons can induce. Figure 2 shows data from reference 5 for wavelengths down to 870 A together with data from reference 6 for the range from 1,300 A to 60 A. Table II gives the integrated intensities, in terms of both photon flux and energy flux, of several bandwidths of the curve from reference 6. The fluxes of Lyman-α radiation of hydrogen (1,216 A) and of singly ionized helium (304 A) are also given in the table.

Table II also shows some similar data from reference 7, obtained 7 months after the data of reference 6 were obtained, by the same investigator. In reference 7 it was noted that there were some appreciable differences between the two sets and it was remarked that the differences may not necessarily reflect merely an improved technique but may be genuine, associated possibly with the fact that the second set of data was obtained at a later time during the present period of solar decline.

It should be mentioned that the spectrum of reference 5 has been deliberately washed out to correspond to an effective slit width of 10 A, in order to provide the comparison with the other spectrum. The original data showed and identified a large number of spectral lines. Solar emission lines, together with their identification, are also given in references 8, 9, and 10.

At the higher satellite altitudes, the residual atmosphere above the satellite does not appreciably attenuate the solar spectrum. At the lower satellite altitudes, there will be appreciable absorption below 900 A, where ionization of the atmospheric constituents commences. Figure 3 shows the absorption curves that were used in reference 6 to apply to the measurements in order to derive the corrected (above the

atmosphere) spectrum shown in figure 2. Note that, since the solar zenith angle was about 60° at the time of the measurement, the total number of molecules in the absorbing column, per square centimeter, is twice the number in a vertical column. Absorption coefficients for the atmospheric constituents are given in references 6, 11, 12, and 13. By means of these data and whatever model atmosphere one wishes to use, one may calculate an absorption curve such as that shown in figure 3 for any specified satellite altitude and solar zenith angle.

As already suggested, the intensities of the emission lines in the far ultraviolet cannot be assumed constant, although thorough data on this subject are not yet available. Emphasis has been laid on the intensity of the hydrogen Lyman-α line at 1,216 A, for which the most recent measurements (ref. 10) consistently give about 6 ergs-cm^{-2}-sec^{-1}. Measurements made between 1950 and 1954 consistently gave values that were considerably lower, one as low as 0.1 erg-cm^{-2}-sec^{-1}. Although the more recent data are presumably obtained with the more sophisticated instrumentation, there is no clear justification for discarding the earlier data, and further correlation between Lyman-α intensity and solar activity will be obtained during the presently developing period of solar decline. Three significant experiments may be mentioned in this connection, however:

(1) A photograph of the sun in the light of the Lyman-α line showed that most of the Lyman-α radiation came from areas that correlated almost perfectly with CaK plages observed simultaneously from the ground. Since the calcium plages tend to disappear at solar minimum, the Lyman-α plages would be expected similarly to disappear at solar minimum, leaving a total solar Lyman-α emission of only about one-fifth of the recent values.

(2) Explorer VII (1959 Iota) provided occasional measurements of solar Lyman-α intensity. The intensity appeared to be constant within about ±20 percent.

(3) Measurements made during classes 1+, 2, and 3 flares gave no evidence for large increases in Lyman-α intensity. The measurements were made only near the times of flare maximum, however, and the possibility that an increase occurs near the commencement of the flare cannot be ruled out.

X-Ray Spectrum

The spectral region below 100 A may be considered the X-ray region. As so defined, the region includes the hump developing at the left-hand end of the curve of figure 2(b), which can be interpreted roughly as thermal radiation from the solar corona at temperatures of the order of

5×10^5 degrees K. Naval Research Laboratory data obtained during the past decade by means of ionization chambers provide further information in this same wavelength range and have also extended the range down to the region near 1 A.

In the years near solar minimum, the energy between 44 A and 100 A is about 0.06 erg-cm^{-2}-sec^{-1}, and if the 44-100 A region is considered to be only part of a black-body X-ray spectrum with peak around 50 A, the total energy of this complete spectrum would be nearly twice this value, or 0.11 erg-cm^{-2}-sec^{-1}. At solar maximum, the X-radiation from the quiet Sun may be nearly 10 times these values, with roughly the same spectral distribution, at least in the neighborhood of the peak (ref. 11). Toward the shorter wavelengths, below 20 A, the energy is still more sensitive to solar activity, but the amount of energy involved is far smaller than the values just mentioned. The total energy (from the quiet Sun) below 20 A has been measured as low as 0.0004 erg-cm^{-2}-sec^{-1} near solar minimum and as high as 0.018 erg-cm^{-2}-sec^{-1} near solar maximum. The spectral distribution in the region just below 20 A resembles that of a 2×10^6 degrees K black body. For the region below 8 A, corresponding values (from the quiet Sun) are 3×10^{-6} and 3.5×10^{-4} ergs-cm^{-2}-sec^{-1}, respectively.

During solar flares, the solar X-radiation increases considerably, especially toward the shorter wavelengths, where the spectral distribution approximates that of a 5×10^6 degrees K black body. The following table lists, for comparison, some measured radiation intensities for a quiet Sun at solar minimum and solar maximum, a class 1 flare, a class 2 flare, and a class 2+ flare (also near solar maximum).

Date	Flare	X-ray flux, erg-cm^{-2}-sec^{-1}			
		20-100 A	8-20 A	2-8 A	0.6 A
11/25/53				3×10^{-6}	
12/1/53		0.10	0.0004		
7/20/56	1; no SWF[a]			.005	
8/29/57	2; $\frac{1}{2}$ hr SWF[a]			.02	
8/14/59[b]		.6	.018	.00035	
8/31/60[b]	2+	<4.0	>.09	>.03	0.000023

[a]SWF is short-wave fadeout.

[b]These data are from reference 14.

The energy distribution in the range below 0.6 A is discussed in detail in reference 15. Photon energies up to 70 kev were measured. Some observations of high-energy photons made during quiet-Sun conditions (ref. 11) indicate differential fluxes of the order of 0.1 photon-cm^{-2}-sec^{-1}-kev^{-1} near 20 kev, 0.01 near 150 kev, and 0.001 near 300 kev, corresponding to a total energy flux in this range (20-300 kev) near 10^{-6} ergs-cm^{-2}-sec^{-1}. In reference 16 is reported a case in which a greatly increased flux of 200-500 kev photons was observed. The radiation was observed about one-half minute before the beginning of a class 2 flare, lasted not over 18 seconds, and had an average intensity estimated at 2.6×10^{-4} ergs-cm^{-2}-sec^{-1}. Absorption of X-rays by the residual atmosphere above usual satellite altitudes is negligible, so that the preceding data may generally be applied directly in determining the satellite environment. For unusually low, short-life orbits, or for conditions in which the Sun is close to the horizon, however, the atmospheric absorption can become substantial. It can be computed from the atmospheric composition and from absorption data in reference 11.

EARTH REFLECTION AND EMISSION

In addition to being subjected to direct radiation from the Sun, an earth satellite is also subjected to solar radiation reflected from the Earth and to the Earth's thermal radiation. The reflected solar radiation covers the same wavelength range as the direct solar radiation, and is hence negligible, at least for satellite thermal problems, beyond 4μ. The Earth's thermal emission has a quite different range, with its maximum intensity in the region of 10μ and with negligible intensity below 4μ. Thus, these two components of satellite irradiation are distinctly separable; nevertheless they are related since both depend on the features of the terrain, the atmosphere, and the weather.

Most of the recent studies of the Earth's albedo (the fraction of intercepted radiation reflected back into space) estimate its average value as about 35 percent. The remaining 65 percent is absorbed and reemitted as thermal radiation. To a first approximation one might consider these two factors to be constant and uniform over the Earth, the reflected radiation to obey the Lambert cosine law and to have the same spectral distribution as the incident solar radiation, and the emitted thermal radiation to have the same distribution and intensity as if the Earth were a black body at a temperature of 251° K. Such approximations are probably adequate for most purposes. Nevertheless, dissatisfaction is occasionally expressed with this simplification; and cases will doubtless arise in which a more precise evaluation of these radiations will be desired. The following discussion is intended to indicate what might be involved in such a more precise evaluation. It will be seen that, in

any case, the radiations are not uniquely definable except at a particular time, although it would not be unreasonable to seek practical upper and lower bounds.

Reflection of Solar Radiation by the Earth

Rayleigh scattering.- Clean dry air scatters light (Rayleigh scattering) approximately inversely as the 4th power of the wavelength and with angle dependency proportional to $1 + \cos^2\theta$, where θ is the scattering angle. Because of repeated scattering within the atmosphere and attenuation of the incident beam due to the scattering itself, the variation with wave length of this component of the albedo is actually less than that corresponding to the inverse 4th power. References 17 and 18 present extensive calculations of Rayleigh scattering. Figure 4 (from ref. 17) shows this theoretical reflectance of the atmosphere (that is, the fraction of incident light that is scattered out of the atmosphere) as a function of wavelength and incidence angle, and also shows the net reflectance of atmosphere and ground when two different values (0.25 and 0.80) are assumed for diffuse (Lambert) reflectance of the ground. These calculations were based on somewhat idealized assumptions. One assumption in particular - that the Earth is flat - results in underestimation of the incident-beam path length for some of the lower solar elevation angles and thus in appreciable underestimation of the reflectance for these cases. From this figure it is apparent that most terrain (surface reflectance between 0.05 and 0.25) will appear bluish when viewed from above the atmosphere, while the whiteness of snow-covered areas (surface reflectance up to 0.9) will hardly be affected. As an example of the application of this figure, a reflectance curve was found, by interpolation, corresponding to a Sun elevation angle of 30° and a ground reflectance of 0.1; and the solar spectrum of figure 1 was multiplied by this curve. The result is shown as the bottom spectrum in figure 1. Comparison with the solar spectrum shows the relative enhancement of the shorter wavelengths.

The middle spectrum of figure 1 is also for a Sun elevation angle of 30° but is for a complete overcast, with the cloud tops at 11,000 feet and an average cloud reflectance of 0.50. Only two-thirds of the atmosphere now lies above the clouds, so figure 4 could not be used directly. Instead, since the effect of air scattering depends on the product (atmospheric depth) $\times$ (wavelength)$^{-4}$, each wavelength was increased by the factor $(3/2)^{1/4}$ before proceeding to figure 4 and interpolating for the desired Sun elevation angle of 30° and ground reflectance of 0.5. This spectrum also shows an appreciable enhancement of the blue. Balloon observations of the effect are reported in reference 19.

In a sense, the 30° elevation angle used in the preceding computations represents an average of the solar elevation angle over the entire

sunlit hemisphere. Thus, since the Earth intercepts a beam of cross-section πR^2, whereas the area of the sunlit hemisphere is $2\pi R^2$ (where R is the radius of the Earth), the average illuminated area receives only half the irradiation of a surface that is normal to the beam; that is, the average sine of the elevation angle is 1/2. However, the results shown in figure 1 are only illustrative and are not intended to represent theoretical average reflections from clear and overcast areas.

The angular distribution of this theoretical scattered and reflected radiation is not uniform. In general, from a point near the top of the atmosphere, the region vertically below would appear considerably less bright than the horizons - simply because the airpath is longer in the latter case. The effect is illustrated in figure 5, from reference 17, which shows the angular distribution of this theoretical scattered and reflected radiation for $\lambda \approx 5{,}000$ A, a solar elevation angle of 53°, and a diffuse ground reflectance of 0.25. The relative difference is even greater for less ground reflectance. It is also greater for longer wavelengths, so that the horizon is not only brighter but also whiter than the vertical.

Two experimental surveys of the visible radiation directed outward from the Earth are shown in figure 6, for comparison with the theoretical angular distribution of scattered and reflected solar radiation shown in figure 5. Figure 6(a), from reference 17, is a survey from a balloon at an altitude of 98,000 feet (obtained by V. J. Stakutis), which is above most of the atmosphere. There is a strong resemblance to figure 5 but the strong scattering from the general direction of 0° azimuth is a definitely dissimilar feature. It is presumably due to haze, as discussed in the following section. Figure 6(b), from reference 20, is a survey from 20,000 feet, which is above half the atmosphere and all the haze. It shows much less of the forward light scattering.

Scattering due to dust and water vapor.- Dust in the atmosphere also scatters light. High humidity similarly results in a hazy atmosphere, possibly because of droplets formed by deliquescent salt particles.

This scattering due to dust and water vapor is much less a function of wavelength than is the Rayleigh scattering. Studies have indicated that in a fairly clear atmosphere, the scattering by dust and water vapor varies roughly as the inverse first power of the wavelength, corresponding to particle sizes about equal to, or somewhat less than, the wavelength of light (ref. 21). For particles appreciably larger than the wavelength of light, the scattering is almost independent of wavelength. An exact theory of this scattering exists for spherical particles, with only imprecise application to dust. Absorption by dust is normally negligible, unless it is smoke.

The angular distribution of the light scattered by dust and water vapor is also quite different from that of Rayleigh scattering. The intensity of forward scattering (within a few degrees of the solar beam) may be as much as a hundred times the intensity of the light scattered at right angles or rearward. There is considerable quantitative variation, however, among the results of different studies. In any case, the very intense forward scattering decreases rapidly with increasing angle from the direct solar beam, so that the total radiation scattered in the forward hemisphere may be only 2 to 5 times as much as that scattered in the rearward hemisphere (ref. 18).

For computational purposes, dust over land, for the Sun at the zenith, has been considered to scatter about 1.25 percent of the radiation rearward and 2.5 percent forward (ref. 22). For the Sun at other elevation angles these numbers are increased inversely as the sine of the elevation angle. For the smaller elevation angles, relatively larger proportions of the total are scattered out of the atmosphere since part of the forward-scattered radiation is included. However, there are few quantitative data on this scattering. Dust over the oceans is generally considered negligible.

For the scattering due to water vapor, 2 centimeters of precipitable water in the atmosphere with the Sun at the zenith may be considered to scatter about 1.25 percent of the radiation rearward and 3.75 percent forward. The amounts are proportional to the water content of the air, and the effects of elevation angle are as just discussed for dust scattering. Scattering by dust and water vapor above the clouds is negligible except perhaps for very low Sun elevation. However, for scattered clouds where, say, half of the incident sunlight passes diffusely through each cloud, the air scattering and ground reflection of this transmitted portion of the sunlight also contributes to the albedo.

Figure 7 shows the spectrum, determined according to the preceding discussion, of the light scattered out of the atmosphere by the dust and water vapor (assuming 2 centimeters of precipitable water in the atmosphere) for the Sun at 30° elevation.

Absorption due to ozone, oxygen, carbon dioxide, and water.- Absorption due to ozone (ref. 23) essentially eliminates all wavelengths between 2,000 A and 3,000 A from the reflected radiation. At 3,200 A, 3,300 A, and 3,400 A, the ozone absorption multiplies the albedo by factors of about 0.4, 0.85, and 0.97, respectively, for the Sun at an elevation angle of 30°. Ozone also has a weak broad absorption across the visible part of the spectrum beyond about 0.45μ, with its peak at 0.6μ. At the peak the corresponding reduction factor is about 0.88 for a 30° elevation angle. These factors are based on a total of 0.25 atm-cm of ozone in the atmosphere, and take into account that the solar radiation

must pass through twice this amount on its way into the atmosphere (because of the 30° elevation angle) and must pass through it again on its way out of the atmosphere.

Oxygen and the remaining atmospheric constituents absorb the radiation below 2,000 A, thereby preventing any appreciable albedo for the far ultraviolet end of the spectrum. As was shown in figure 1, the low infrared intensities (compared with the visible) of the solar spectrum and the strong preferential scattering of the low-wavelength end of the spectrum combine to reduce greatly the relative intensity of the infrared in the clear-sky reflected radiation. Water absorption bands and a few less intense carbon dioxide bands carry the process further by removing practically all of the radiation above 2.5μ and considerable sections of the spectrum below 2.5μ.

The reflected radiation indicated in figure 1 for the condition of complete cloud cover shows much less of the preferential reflection of the low wavelengths. Nevertheless, because of the strong absorption of the infrared by liquid water and also by the saturated water vapor within the clouds, much of the infrared is removed for this case too. Quantitative data on this absorption, however, are not available, but some theoretical calculations are given in reference 24.

Corrected reflection spectra.- By means of the preceding corrections for absorption, the two reflection spectra of figure 1 and the additional reflection spectrum of figure 7 have been corrected to the spectra of figure 8 and the dotted spectrum of figure 7, respectively. For a completely overcast sky, the upper curve of figure 8 represents the entire reflected radiation; for a completely clear sky the reflected radiation is approximately the sum of the lower curve of figure 8 and the dotted curve of figure 7. These curves are, of course, only estimates and, in any case, correspond only to two particular sets of conditions; nevertheless they are considered to be fairly representative.

In the following two sections is given a brief review of reflectance data for different surfaces, for use in applying the results of references 17 and 18 and also to indicate how closely the angular distributions of reflectance obey Lambert's law.

Ground and cloud reflectance.- Figure 9, from reference 25, is a schematic reflectance curve for the higher chlorophyll-containing plants. It is reasonably typical of deciduous forests or of green fields. Dark, dense (as conifer) forests may show a roughly similar curve with the ordinates reduced uniformly by a factor of 2. There are, of course, variations with season. Soils have reflectances of about 0.03 to 0.08 in most of the visible, with an increase to perhaps 0.25 in the infrared just beyond the visible. The reflectance of sand is between 0.10 and 0.18 at $\lambda = 0.4\mu$, rises through the visible to values between 0.25

and 0.45 at $\lambda = 0.7\mu$, and may rise further to 0.5 to 0.7 in the infrared just beyond the visible. Prairies, steppes, tundras, scrublands, deserts, and so forth have reflectance characteristics that consist of various proportions of the characteristics just described.

The reflectance of fresh snow is 0.83 to 0.90 at $\lambda = 0.4\mu$ and decreases gradually to about 0.6 at 0.9μ. It drops sharply at 1.5μ and is practically zero beyond 2.0μ. Older snow has less reflectance, depending on how dirty or crusty it has become.

The reflectance of the whitest clouds may be as high as 0.80 in the visible, but, because of absorption by both water and water vapor, it drops gradually beyond the visible to about 0.5 at 2.5μ. Less dense clouds, or clouds containing larger droplets, will have less reflectance. The average reflectance of unspecified "clouds" is commonly taken as about 0.50.

Reflectance values such as those given in the preceding discussion are, of course, only approximate, not only because the surfaces are not very well defined but also because the values depend on the angle of incidence of the incoming radiation. Of at least equal significance is the fact that the angular distribution of the reflected radiation does not, in general, even approximately satisfy Lambert's cosine law. It is well known that a rough surface, whether it be a bed of gravel or a mountain range, reflects light most strongly back toward the general direction of the source; and very little light is reflected toward the mirror-reflection direction, simply because the rear slopes of the roughnesses are only slightly illuminated or may even be in shadow. Sandy surfaces generally also show this effect, although some white sands tend to show the opposite effect. Forests and fields are like rough surfaces in this respect, but their reflection characteristics may also be influenced by winds. As an example of the vagaries of reflectance characteristics may be mentioned the observations of a wheat field (ref. 26) with the Sun at an elevation angle of 40°, for which there was strong reflection back toward the source and also in the general mirror-reflection direction, but almost no reflection toward the vertical. Fresh snow is a reasonably Lambertian reflector, but older crusty snow is more like a rocky surface. Reference 26 is a basic source of data of this nature. Reviews of this and other sources are in references 17 and 23.

Of the estimated value of 0.35 for the Earth's albedo, about 0.25 is due to the clouds that, on the average, cover half of the Earth's surface. The directional characteristics of cloud-top reflectance have not been thoroughly explored. One might suppose that, because of the characteristic lumpy structure of the top of an overcast, the situation would be similar to that of a rocky surface for which, with the Sun at a fairly low elevation angle, most of the light is reflected back toward

the source. Actually, the opposite is more common for such a cloud top, doubtless because of the intense forward scattering from the water droplets. (In addition, for fairly obvious similar reasons, the reflectance of thin clouds is much higher for low than for high Sun elevation angles.) On the other hand, heavy cumulus-type pillars and cauliflower-head formations do reflect sunlight more strongly back toward the source.

Water reflectance.- The oceans are of particular interest since they cover more than two-thirds of the Earth's surface. Fresnel's theoretical formula for the reflectance of a smooth glass or liquid surface is not directly applicable to a wavy and choppy ocean surface. Furthermore, some of the incident radiation is diffusely reflected by bubbles, suspended particulate matter, and water molecules; also, reflection of skylight adds an additional diffuse component to the reflected radiation. In figure 10 are plotted calculated reflectances (from ref. 27) of smooth and rough water for combined direct sunlight and skylight under minimum-haze conditions, as a function of solar elevation angle. These calculations are shown in reference 27 to be in good agreement with the experimental measurements of reference 28.

A typical directional distribution of the reflected solar radiation from the sea is indicated qualitatively in figure 11 (from ref. 29), which is an aerial photograph of the Pacific Ocean under a 9-knot wind, with the sun at 50° elevation. The peak intensity is roughly at or somewhat beyond the mirror point (the center of the grid). The path of the reflected sunlight along the water extends forward almost to the horizon (although it would not for higher elevation angles) but extends backward from the mirror point only about 20° to 25°; also, it extends only about 20° to 25° to either side of the plane of incidence.

Occasionally a satellite will catch an almost specular reflection of the Sun from a quiet body of water. Such occasions are too rare and too fleeting to be of any significance with regard to thermal balance, but they might affect an optical experiment. Figure 12 is a Tiros I photograph showing such a reflection of the Sun in the Aral Sea. More typical satellite photographs, in which bodies of water appear as the darkest areas of the photographs, are shown in reference 30.

The Earth's albedo from statistical meteorological data.- The preceding two sections have indicated part of what may be involved in attempting refined calculations of the solar radiation reflected by the Earth to a satellite. About the closest approach to such work is that of the meteorologists in their studies of the atmospheric heat balance. Reference 22 may be cited as a single source containing much of the relevant meteorological data (for average conditions) on which the estimates are based, along with discussions of the procedures and results. It gives latitudinal and seasonal distributions of total cloudiness, of the amount and height of various cloud types, of the incoming solar

radiation at the top of the atmosphere, and of the radiation reflected back to space. It also contains data on latitudinal distribution of ground albedo and charts of the geographical and seasonal distribution of total cloudiness in the northern hemisphere. Data on the reflectances of different types of clouds and ground are also given. Most of the statistical-average data apply specifically to the northern hemisphere. Less is known of the southern hemisphere, but its average cloudiness is considered to exceed that of the northern hemisphere. On the whole, reference 22 shows very little variation of the Earth's albedo with season, but it does show relatively low average albedos (27 percent) in the subtropics and high values (45 percent) in the higher latitudes.

In spite of the thoroughness of the studies in reference 22 and in similar papers (refs. 31 and 32), and in spite of the previously indicated fairly large amount of data on reflectances, the extreme design conditions for a satellite thermal analysis are not yet accurately defined. Low local albedos could exist over most of the sunlit areas under an orbit if the areas are mostly ocean and forest, with clear skies and low humidity. High albedos could exist if most of the sunlit areas are fresh snow or clouds. However, no studies are yet available that indicate the likelihood of such conditions or that specify statistically reasonable extreme proportions of these two types of areas that might exist for a single orbital pass or for several successive passes. Even with such studies, it would still be desirable, in a refined thermal analysis, to take into account the directional characteristics of reflectances. It might be suggested that, for low latitude (subtropical) orbits, a cloudless condition and a 50-percent-cloud condition be taken as extreme design conditions, and that, for the higher latitude (say 60°) orbits, 25-percent- and 75-percent-cloud conditions be used.

Studies of the earthlight on the Moon.- Measurements of the Earth's albedo have been made by means of visual observations of the earthlight on the Moon (ref. 33). Values for the visual albedo between 32 percent and 52 percent were found, with the average about 40 percent (which, with estimated adjustments for ultraviolet and infrared absorption, is reduced to 36 percent for the total albedo, in good agreement with the meteorologists' estimates). The angular distribution of the reflected radiation from the Earth, as derived from these measurements, is given in figure 13.

The lowest visual albedo, 32 percent, was the average for both July and August; the highest, 52 percent, was the average for October. Since the observations of the Moon were made from France, any clouds over the Pacific Ocean could not contribute to the observed earthlight; furthermore, the latitudinal distribution of cloudiness might easily be such that the solar radiation reflected from the Earth is not symmetrical about the Earth-Sun axis (which symmetry was assumed in determining the

albedo in ref. 33). Thus the nearly constant Earth albedo derived in reference 22 is not necessarily in essential disagreement with the observations of the earthlight on the Moon.

Thermal Radiation From the Earth

Basic principles.- Most types of terrain, including snow and water, are considered to radiate essentially as black bodies in the infrared. Since laboratory tests of various materials frequently show emittances of the order of 0.8 to 0.9, this common assumption may be taken as too high by about 10 percent. As will appear later, the difference usually matters very little. Clouds are also considered to radiate as black bodies. The thermal radiation going out into space from any part of the Earth, however, is only partly related to the temperatures of the tops of the clouds or of the ground in that area. The reason is that the carbon dioxide, water vapor, and ozone in the atmosphere have strong absorption bands in this infrared range and profoundly affect the radiation leaving the cloud top or ground.

Carbon dioxide has an absorption band extending from about 12μ to about 18μ, with its peak at 14-16μ. The carbon dioxide in the atmosphere causes even the air in the stratosphere to be essentially black in the neighborhood of this peak, so that the only 14-16μ radiation going off into space has the intensity corresponding to a black body at stratosphere temperatures. Near the edges of the band, the absorption band is much less intense; however, its effect is enhanced by the fact that energy is radiated not only vertically through the atmosphere but also at oblique angles, so that the mean effective path length of the radiation through the stratosphere is considerably greater than the thickness of the stratosphere. As a result, the main part of the radiation in this range going off into space corresponds to a temperature of about 230° K.

The atmosphere has a "window" between about 8.3μ and 12.5μ where it is fairly transparent. The radiation going off into space within this range, however, corresponds only approximately to the ground temperature or to the temperatures at the tops of the clouds because:

(1) The dust and water vapor (haze) in the air at the low altitudes are partially absorbent.

(2) The molecular water and the carbon dioxide in the air have absorption bands adjacent to the window, and some weaker absorptions within the window. With high absolute humidity or with slant viewing, the wings of the bands extend with appreciable intensity into the window. This item is perhaps not clearly separable from item (1). The effect of both items is that a temperature about 15° C below ground temperature is frequently a more accurate value than ground temperature itself for the effective radiation temperature in the window region.

(3) The ozone in the air has an absorption band about 1μ wide, centered at 9.6μ. The ozone concentration in the stratosphere is not quite enough to make it black in this infrared band. Accordingly the radiation escaping in the 9.1-10.1μ range is roughly midway between that corresponding to ground temperature and that corresponding to stratosphere temperature. The radiation escaping obliquely out of the atmosphere corresponds more nearly to stratosphere temperature. The ozone effect is complicated by the fact that the ozone distribution in the atmosphere is, like the water-vapor distribution, variable with time; however, since the variation is not very large, and since the ozone effect is fairly small, the variability is not generally considered in radiation calculations.

(4) The fact that sandy areas have low emission in the 7.5-9.5μ range will still further lower the level of the window radiation over many areas of the earth.

At wavelengths less than that of the window, molecular water has a series of strong absorption bands extending down to the lower end of the wavelength range of interest. The water vapor content of the atmosphere drops rapidly with increase in altitude, but with sufficient information one may determine an effective radiation temperature for this part of the spectrum. Computations usually show it to be the temperature a few thousand feet below the tropopause. Again, for obliquely escaping radiation the temperatures at a slightly higher altitude would be used.

The region beyond 18μ contains water rotation bands that become progressively more intense with increasing wavelength. The region from 17.5μ to 23μ contains the low-intensity end of the previously mentioned carbon dioxide band and the beginning of the water band, and thus also constitutes an approximate window. For a clear sky, the vertically outgoing radiation in this region corresponds to the temperature at an altitude of 5,000 to 10,000 feet (depending on the absolute humidity) while the vertically outgoing radiation near 40μ corresponds to temperatures near 25,000 feet.

Examples of calculated thermal-radiation spectra.- In references 34 and 35 extensive radiosonde data (covering atmospheric temperature and humidity up to high altitudes) for a given date were analyzed along the lines indicated in the preceding discussion in order to map the vertically outgoing radiation over the United States. The results were presented in the form of tables and contour maps of effective radiation temperature within certain bands or wavelength intervals. From these results two block-type spectral distributions, shown in figures 14 and 15, have been plotted. Figure 14 is for the neighborhood of Norfolk, Va; figure 15 is for the neighborhood of Miami, Fla. There were very high clouds over Norfolk on that day, so that the window radiation in the 8.3-12.5μ region corresponds to the temperature at the top of the clouds. The radiation

in the 9.1-10μ ozone band is seen to be more intense than the window radiation, contrary to the previous discussion. This increased intensity occurs because of the increased temperature in the standard temperature-altitude and ozone concentration-altitude curves that were used in these calculations. The weather at Miami was clear, so that the window radiation in figure 15 corresponds to a fairly high temperature. The radiation in the ozone band is now less intense than the window radiation, as predicted in the earlier discussion. The intensities in the 15μ carbon dioxide band and in the water band beyond it are in agreement with the previous discussion of these regions.

The areas under the Miami and Norfolk spectra correspond to 0.439 and 0.202 cal-cm^{-2}-min^{-1}, or 305 and 141 watts-m^{-2}, corresponding to effective black-body radiation temperatures of 271° K and 223° K, respectively. Other calculations (ref. 36), for typical conditions at various locations in the northern hemisphere, have given clear-sky values between 274 watts-m^{-2} (for Broken Arrow, Okla., in summer) and 164 watts-m^{-2} (for Buchta-Tichaja, Franz Josef Land, in winter), and overcast-sky values as low as 114 watts-m^{-2}.

The two spectra and these radiation fluxes illustrate the deviations from the simple 251° K black-body radiation that corresponds to the average energy emission from the Earth. It will be recalled also that even at a particular point at the top of the atmosphere the outgoing Earth radiation is not directionally uniform, since the radiation from near the horizons contains less of the window radiation and, in general, corresponds more closely to the temperatures in the stratosphere (about 200° K near the equator and 225° K near the poles).

Satellite data.- Of the Explorer VII data, only some preliminary thermal-radiation maps have been thus far published (refs. 37 and 38). From these, one might suggest that the average thermal radiation received during, say, half an orbit may be as high as 0.39 cal-cm^{-2}-min^{-1} (tropical) or as low as 0.31 cal-cm^{-2}-min^{-1} (high latitudes). Extensive numerical data (spectral and total) obtained with the Tiros II satellite have just been made available (ref. 39), but they have not yet been thoroughly studied along the lines here indicated.

LIGHT IN THE NIGHT SKY

The present section will briefly review various lesser radiations to which a near-Earth satellite would be subjected. Moonlight will not be discussed here since it will be treated in the following section.

Starlight

A contour map of the distribution of starlight over the celestial sphere is given in figure 16 (from ref. 40). A more recent tabulation is given in reference 41. These data refer only to the light from stars weaker than sixth magnitude, and accordingly account for only about 0.8 of the total starlight. Reference 13 contains additional statistical data on starlight. The map in figure 16 shows the distribution of visual intensity. The photographic intensity is only about half as much; that is, average starlight is redder than sunlight. The intensity of the total starlight falling on a space vehicle is estimated as about 0.008 ergs-cm^{-2}-sec^{-1}. The corresponding "effective temperature" of interstellar space is about 3° K; but this temperature corresponds to the energy flux and not to the spectral distribution, which is not at all similar to that of a 3° K black body (ref. 13).

Night Airglow

Most of the energy in the visible airglow is due to lines at 5,577 A, 5,893 A, and 6,360 A; however, there are other lines in the visible and bands extending down into the ultraviolet. The dominant 5,577 A line originates in a layer about 25 kilometers thick, with the peak intensity at an altitude of about 85 to 95 kilometers; thus it will irradiate even a low-altitude satellite mainly from below, and should be visible from a satellite as a bright band on the horizon. The weaker red lines probably originate at altitudes of about 250 kilometers and above. For a satellite orbiting somewhat above this altitude, the total intensity in the visible (say up to 7,200 A) striking it from below is about 0.002 erg-cm^{-2}-sec^{-1}. The intensity from 0.72μ to 1.0μ is about 0.05 erg-cm^{-2}-sec^{-1} (most of which is not detectable from the ground because it is absorbed by molecular oxygen). A band from 1.0μ to 1.33μ contributes about 0.06 erg-cm^{-2}-sec^{-1}; and a band from 1.46μ to 1.86μ contributes about 0.3 erg-cm^{-2}-sec^{-1}. Bands from 2.0μ to 4.5μ probably also contribute about 0.3 erg-cm^{-2}-sec^{-1}; this energy, however, is now small compared with the thermal radiation from the Earth in this spectral range, and would not be easily detected unless the observation is directed tangentially along the airglow layer.

At times of solar activity the intensity may become as much as four times the normal intensity, and the spectral distribution is also modified. In addition, there are characteristic variations of the spectral content and intensities as a function of solar time during the night (ref. 42). Artificial illumination from the industrial territories of the Earth can also illuminate the satellite from below with an average intensity of the same order as the airglow, but with occasional much higher intensity. Thus, a city will appear as bright from a satellite as from an airplane, although its subtended angle will be smaller.

Night Lyman-α

Night Lyman-α radiation, with a flux density of about 0.01 erg-cm^{-2}-sec^{-1}, originates in a hydrogen geocorona that extends out to about four Earth radii. The atmospheric albedo for this radiation is about 42 percent, so that a satellite will also be exposed to Lyman-α radiation from below (ref. 11).

Auroras

The aurora might be mentioned as an additional source of night radiation in the neighborhood of the visible and near infrared. A strong solar flare might produce, after a day or so, a bright high aurora in the middle or high (geomagnetic) latitudes, extending laterally a thousand miles or more. A satellite in a middle-latitude orbit passing along such an aurora might be bathed for several minutes in light of intensity comparable to that from the full Moon. The high-latitude auroras are more commonly at somewhat lower altitudes (mainly below 135 kilometers) so that most satellites will be above them. In any case, such bright auroras are relatively rare, especially in the middle latitudes, but the weaker ones are fairly common in the higher latitudes, and in regions about 20° from the geomagnetic poles practically every night has a discernible aurora (ref. 43).

Twilight

Because of atmospheric refraction, some direct solar radiation can (unless high clouds or mountains intervene) strike an Earth satellite when the Sun is slightly more than 1° below the geometrical horizon; or, in general, light from any point on the Sun will, on passing through the different layers of the Earth's atmosphere, be spread out into a 1° fan. The sunlit portion of the orbit will thus extend slightly beyond the limits predicted from purely geometrical considerations; for certain cases, as for orbits strongly inclined to the ecliptic, these extensions may be several degrees long.

Atmospheric absorption and scattering, however, will strongly attenuate the solar radiation along these extensions. In the rays passing through the lower part of the atmosphere, practically none of the blue end of the spectrum would be transmitted, and even the red would be attenuated by a factor of many thousands.

With the Sun just below the apparent horizon, atmospheric scattering will produce an illuminated twilight arc extending up to a height of 30 or 40 kilometers. The glow is about gone when the Sun is 10° below the

horizon, although measurable multiply scattered light can be transmitted around several degrees more.

The twilight is mentioned here mainly to point out that near the ends of the nominal shaded part of its orbit a satellite of the Earth, Venus, or Mars will not quite be in typical nocturnal darkness. Further discussion of the basic factors involved may be found in reference 21 and in the references therein cited.

Solar Corona

Another source of radiation that one may, in rare cases, wish to consider for the periods when the Sun itself is just below the horizon is the solar corona. Various observations of the corona have shown, in addition to the characteristic streamers, gross and sporadic asymmetries and irregularities. For the following brief review, based on reference 13, these have been averaged out. The (average) corona has approximate radial symmetry at solar maximum. At solar minimum its brightness along the equator is of the order of twice its brightness along the poles.

At solar maximum, the total coronal light flux outside of 1.03 Sun radii is about 1.3×10^{-6} the solar flux; at solar minimum it is about 0.8×10^{-6} the solar flux. These numbers are about 0.57 and 0.35 as much, respectively, as the flux received at the Earth from the full Moon. The coronal brightness decreases rapidly with distance from the Sun (fig. 17), so that 98 percent of the flux is received from the region within one solar radius of the solar disk. The spectral composition of the coronal radiation is roughly the same as that of the Sun. It would seem, from these data, that only for a Moon satellite could the corona ever provide a significant fraction of the total illumination; for a satellite of the Earth, Venus, or Mars, its light would be submerged in the sunlight refracted and scattered by the atmosphere.

Zodiacal Light

The equatorial extension of the corona merges into the zodiacal light, a nebulous band of luminosity along the ecliptic with intensity that decreases rapidly with increasing angular distance from the Sun. Its spectral composition is about the same as that of sunlight. The intensity along the center of the band is plotted in figure 17 (mainly from ref. 44); and the distribution of intensity across the band is indicated by the intensity contours of figure 18, from reference 45. The small intensity peak at 180° elongation represents the gegenschein, or counterglow, an oval area of increased intensity about 8° to 10° in diameter. Intensity increases of the order of 50 percent possibly occur at times of increased solar activity (refs. 40 and 44). The integrated

intensity of the zodiacal light, for angular distances from the Sun greater than about 30°, is of the order of one-half that of starlight.

The data of figures 17 and 18 were obtained in Earth-based observations. It might be conjectured that, for the same angular distance from the Sun, the brightness would be about twice as much in the neighborhood of Venus and about half as much in the neighborhood of Mars.

THE MOON

The Moon is involved in the present review first as a possible dominant source of night-sky radiation for an artificial Earth satellite, and second as a main source of the radiation environment of an artificial Moon satellite. Correspondingly, in the following discussion the first part will give data for the Moon considered essentially as a distant undifferentiated source of radiation, and the second part will give more detail on the radiation characteristics of its different areas.

The Moon as a Distant Source

The photovisual magnitude of the full Moon differs from that of the Sun by about 14.08 (ref. 46). That is, in the neighborhood of $\lambda = 5,400$ A, the full Moon as seen from the Earth is about 1/430,000 as bright as the Sun (for the Earth at its mean distance from the Sun and the Moon at its mean distance from the Earth). As shown in figure 19 (from ref. 47), the ratio gradually decreases toward the violet and then drops sharply in the ultraviolet. Other data indicate that the variation is somewhat greater for the continents than for the maria. Some recent studies indicate that the rising trend toward longer wavelengths continues into the infrared.

The "full Moon" as used here is actually a slightly fictitious concept so far as concerns a near Earth satellite, since the Moon would be in eclipse when it is exactly alined with the Sun and the Earth; in fact, the Moon touches the penumbra when it is 1.5° from such collinearity. Data for the full Moon represent extrapolations to zero phase angle.

The variation of total brightness of the Moon with phase angle is given in the following table (based on the data of ref. 48):

Phase angle, deg	Relative total brightness of the Moon														
	0	10	20	30	40	50	60	70	80	90	100	110	120	130	140
Waxing . . .	1.0	0.810	0.616	0.482	0.356	0.281	0.220	0.167	0.121	0.085	0.057	0.039	0.025	0.016	0.0096
Waning . . .	1.0	.750	.572	.445	.342	.264	.204	.148	.105	.078	.058	.041	.027	.017	.0096

Values are given for both the waxing and waning halves of the lunation, since they were found to be different. The brightness decreases with increasing phase angle far more rapidly than if the Moon were a Lambert reflector; or, stated differently, the brightness of the full Moon is far out of proportion to the brightness in the partial phases. Thus, although integrating the moonlight over all directions gives a value of only 7.3 percent for the total reflectance, or Russell-Bond albedo (photovisual), the brightness of the full Moon corresponds to a Lambert sphere with 18.6-percent reflectance or to a Lambert disk with 12.4-percent reflectance. Brightness, as used here, refers to the total light received from the Moon. Dividing by $\frac{1 + \cos \theta}{2}$, where θ is the phase angle, would give the (average) relative brightness per unit illuminated area of the disk.

Figure 20, from reference 49, shows the variation of the brightness during the progress of an eclipse, for two wavelengths. For $2\frac{1}{2}$ hours the brightness was less than 10 percent of that just before the eclipse; and for 2 hours of this period it was less than 1 percent. At the center of the eclipse, the percentages for $\lambda = 5,458$ A and $\lambda = 6,230$ A were 0.003 and 0.005, respectively. These last data, however, must be considered only as representative, since the minimum brightness can vary by at least a factor of 3 and the color can vary from coppery to blood red, depending on conditions in the Earth's atmosphere. The disk is typically darker and redder near the center than near the limb during an eclipse.

Surface Reflection and Radiation Characteristics

Reflection characteristics.- Although many details of the lunar surface have their own peculiar optical characteristics, a set of average characteristics would probably be adequate for a lunar satellite design. At most the satellite designer might wish to consider the surface as a pattern of dark maria and lighter continents, and to differentiate only

between the optical characteristics of these two types of surfaces. Accordingly only these two types will be discussed here. The pattern of maria and continents over the part of the surface visible from the Earth is, of course, well known. The far side of the Moon seems, on the basis of the Lunik III pictures, to be mostly continent.

As has already been mentioned, Lambert's cosine law does not even approximately describe the reflection characteristics of the Moon's surface. The surface brightness observed from the direction of the incident beam is much greater than the surface brightness observed from other directions; furthermore, the intensity of this back reflection is almost independent of the angle of incidence, so that the full Moon appears, in this respect, like a disk rather than a sphere.

Tables III and IV give the (visual) reflectances, relative to that of a white Lambert surface, of maria and continents, respectively, for various angles of incidence and reflection. For these data, taken from reference 50, the incident beam, the reflected beam, and the normal are all in the same plane. In the upper halves of each table the values along the diagonal are for the reflected ray returning along the incident ray. These values are exactly proportional to the secant of the incidence angle, in accordance with the remark at the end of the preceding paragraph. This exact proportionality, however, is more an assumption to help fair the data than a fact proved by the data to within the indicated three-figure accuracy.

A significant indication of the spread of such data is apparent in its deviation from the reciprocity principle (ref. 51). According to this basic law of reflection optics, which must hold for any surface, given any two directions θ_1 and θ_2 from the normal (see sketch),

$$\frac{\text{Surface brightness observed from } \theta_2}{(\text{Intensity of incident beam from } \theta_1) \times \cos\ \theta_1} = \frac{\text{Surface brightness observed from } \theta_1}{(\text{Intensity of incident beam from } \theta_2) \times \cos\ \theta_2}$$

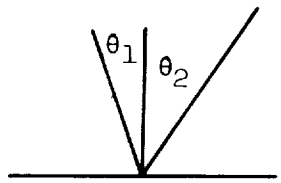

Since the cosine factors in the denominators are already included in the values given in the tables, every value ought to remain the same when i and ϵ are interchanged. Inspection of the tables shows that for many such pairs of values the agreement is quite good but that for many others the disagreement is considerable.

Another discrepancy appears when these data are compared with the previously presented data for the full Moon. It was there stated that the full Moon was 12.4 percent as bright as a white Lambert disk. The reflectances in the tables for normal incidence and reflection are 0.124 for continents and 0.081 for maria. Since the visible disk is about half continent and half mare, the average brightness coefficient should then be about 10.3 percent instead of 12.4 percent. The 10.3-percent value seems to be in much closer agreement with the older studies of Moon brightness in reference 52.

These tables, as already noted, give data only for the cases in which the incident beam, the reflected beam, and the surface normal all lie in the same plane, since they were obtained from measurements on areas lying along the equator. There are no published data for the general case in which the three directions are not coplanar. A possible approach to such information is as follows: In reference 53, it was mentioned that similar areas along the same longitude meridian exhibit the same variation of brightness with phase. A simple geometrical analysis shows that this observation is equivalent to the following statement: Given the reflectance for an incidence angle i and a reflection angle ϵ in the plane of incidence, the same reflectance applies for an incidence angle $i' = \cos^{-1}(\cos \gamma \cos i)$, a reflection angle $\epsilon' = \cos^{-1}(\cos \gamma \cos \epsilon)$, and the same angle $i + \epsilon$ between the incident and reflected rays. The angle γ may have any value between 0° and 90°; it represents the lunar latitude of the reflecting area. As has already been mentioned, the values in tables III and IV have already been divided by $\cos i$; hence, when a value given in the table for (i,ϵ) is applied to (i',ϵ'), it must be multiplied by $\cos i/\cos i'$. Values obtained in the manner just described, for the case in which the plane of incidence is perpendicular to the plane of reflection, are given in tables V and VI for maria and continents, respectively.

Thermal-radiation characteristics.- In reference 54 are given contours of effective thermal-radiation temperatures observed on the sunlit surface of the Moon for a number of different phase angles. From these data, figures 21 and 22 were derived. In figure 21 are plotted contours of the effective radiation temperature as a function of the angle of incidence of the sunlight and the angle of observation of the thermal radiation, for the case in which the direction of observation is in the plane of incidence. As might be expected, the effective radiation temperatures tend to peak where the direction of observation coincides with the direction of incidence. The peak is not as sharp as for the reflected radiation, however (compare with tables III and IV). In figure 22 are

plotted similar contours for the case in which the plane of the observation direction and the surface normal is perpendicular to the plane of incidence.

In the preparation of these two figures no effort was made to differentiate between maria and continents; all of the interesting irregularities in the data were faired out, so that the figures relate only to an average lunar surface. Furthermore, the lunar time of day was not considered as a parameter, although the finite, albeit small, thermal diffusivity of the surface material should result in some temperature lag. From the results of reference 55 for the full Moon it is apparent that the lag is quite small over most of the sunlit face. However, the effect should be appreciable near the terminator; for example, the surface at 5° before sunset is probably of the order of 10° C to 20° C warmer than the surface at 5° after sunrise (ref. 56). Another source of uncertainty in interpreting all the data is that only part of the infrared emission spectrum of the surface is transmitted through the atmosphere and is thus available for measurement. In spite of the basic inaccuracies and incompleteness of the data, the figures are probably adequate for present purposes.

The surface temperature drops from about 215° K where the surface first goes into shadow to 150° K within 5° to 10° beyond sunset and then continues to drop at about 0.3° C per degree of longitude, reaching about 120° K in the middle of the dark side and about 90° K just before sunrise (ref. 55). During an eclipse the temperature of the face toward the Sun also drops sharply, but not as far. In the observations of reference 57, the effective radiation temperature of a point near the center of the disk fell from 371° K to 200° K during the first partial phase and continued to drop to 175° K during totality. At the beginning of totality the temperature was falling at the rate of 30° C per hour but at the end of the first hour the rate was 7° C per hour. The particular significance of lunar eclipses, of which as many as three may occur in one year, is that the Moon satellite may, for a period of 2 or 3 hours, receive essentially no solar radiation and very little thermal radiation from the Moon itself.

In addition to the references already cited, reference 58 should be mentioned as a broad review of the literature on the lunar environment.

Night-Sky Radiation Near the Moon

Starlight and the zodiacal light will be the same for a Moon satellite as for an Earth satellite. There will be nothing equivalent to the Earth's night airglow, auroras, twilight, or Lyman-α radiation from the geocorona. However, the Lyman-α radiation from the Earth's geocorona should be included as a component of the night sky radiation near the

Moon. By far the most important night light will be the Earth, which, at full phase, illuminates the Moon 45 times as brightly as the full Moon illuminates the Earth. This ratio refers to the 5,000-6,000 A wavelength range. Toward the blue end of the spectrum, where the reflectance of the Moon decreases and that of the Earth increases (figs. 1 and 19), the ratio will be larger. The average variation of the brightness of the Earth with phase angle is given in figure 13; however, the brightness at any phase is strongly affected by the weather, specifically the cloudiness, on the sunlit part of the disk.

VENUS

Venus is completely enveloped in clouds so that the observable surface is essentially uniform and undifferentiated. Its visual albedo is between 0.73 and 0.80 (ref. 59), higher than that of any other planet; also the angular distribution of its reflected radiation (see fig. 13) is the most nearly Lambertian. Viewed from the direction of the Sun it is 0.56 as bright as a white Lambert disk, or 0.84 as bright as a white Lambert sphere (if the visual albedo is taken as 0.73). The spectral reflectance, relative to that at 5,500 A, is plotted in figure 23 (refs. 59, 60, and 61). Because of the sharp drop in the blue, the planet is somewhat yellowish. Toward the large phase angles, however, where the relative importance of atmospheric scattering increases, the planet appears bluer, perhaps even bluer than the Sun.

Observations of the night side of Venus have indicated the presence of a uniform night glow, comparable in intensity to moonlight on the Earth.

The effective thermal-radiation temperature at the center of the disk was found (ref. 62) to be 234° K. The observed radiation intensity decreases toward the limb, approximately as $\cos^{1/2}\theta$ (where θ is the angular distance from the center of the disk), so that the average effective radiation temperature of the whole disk is 226° K. These numbers are for the sunlit or mostly sunlit disk; the dark disk is only about 2° C to 3° C colder.

Reference 63 may be mentioned as a broad review of the environment of Venus.

MARS

Features, Weather, Variability

Like the Earth and unlike Venus, Mars exhibits considerable variability of appearance and of optical characteristics. The most conspicuous of the variable features are the white polar caps. In the south they can extend to 42° latitude near the end of winter but evaporate completely by the end of summer; the northern cap does not extend below 55° latitude and seldom disappears completely in summer. The difference is due to the large eccentricity of the orbit, 0.093, which causes the planet to be much closer to the Sun during the northern winter and southern summer than during the northern summer and southern winter. (Perihelion is at heliocentric longitude 335°; southern summer solstice is at 357°. The rotation axis is inclined 24° from the normal to the plane of the orbit.) The caps are apparently H_2O snow, at temperatures probably below 200° K when forming during winter but probably closer to 250° K when evaporating. Their reflectance, as viewed from the Earth, is 0.4 to 0.5 when fresh, and 0.3 to 0.4 when aged.

The atmosphere is characterized, typically, by the so-called "blue haze" or "violet haze," fairly transparent toward the red end of the spectrum (except near the limb, where the optical path length is large), but essentially obscuring the entire surface for wavelengths less than about 4,250 A to 4,500 A, depending on the degree of haziness at the time. On rare occasions, occurring especially near oppositions, the blue haze practically disappears, so that the surface detail is visible at 4,250 A. More often, there exist areas of increased density, or "blue clouds" (visible only through a blue filter), typically over the morning areas, dissipating before noon, and reforming toward evening. There also appear, especially near aphelion, heavier "white clouds" that are visible at all wavelengths below the deeper reds but are most visible in the blue. They are much less white than the clouds of the Earth or Venus but are occasionally as bright as the polar caps. They typically form in the late afternoon. Whitish areas on the sunrise limb, generally disappearing within 2 hours after sunrise, are probably ground frost. The blue haze, blue clouds, and white clouds may all be variations of the same phenomenon - ice condensations in the higher atmosphere.

An entirely different phenomenon is the yellow clouds, considered as dust storms, which are sometimes localized but which have been known to cover the entire planet with a yellow pall for days and, after they subside, to leave some temporary changes in the markings of the planet along with a general reduction of contrast between the darker and lighter areas. The yellow clouds occur most often when the planet is near perihelion. They are not visible in blue light, presumably because the blue haze lies above them; but in yellow they can be as bright as the polar caps.

The surface itself shows a pattern of dark and light areas and bands (refs. 64, 65, and 66), with noticeable variations of brightness, however, among both dark and light regions. The dark areas cover about one-fourth of the southern hemisphere, mostly between the equator and 60° latitude, but cover only about one-fifteenth of the northern hemisphere. They become darker in spring and summer.

Albedo

The planetary albedo is affected by the size of the polar caps and by the weather. Long-term fluctuations of 0.48 magnitude, or 1.56:1, have been indicated (ref. 59), although this value may be too large. Such fluctuations could be due to the polar caps, especially the southern cap, and to the clouds. Each cap makes its greatest contribution to the albedo in spring, when it is near maximum size, the covering mist is partly dissipated, and the polar axis is beginning to incline toward the Sun. The observed brightness should also vary as the planet spins on its axis because of the varying proportions of light and dark regions on the observed sunlit area. Diurnal variations of ±20 percent have been reported in reference 67 (with a filter that transmitted all wavelengths greater than 0.52μ), but other observers (ref. 59) consider half as much to be more likely, at least for the entire sunlit hemisphere.

For normal haze, figure 24 (from ref. 59, based on ref. 68) gives the geometric albedo and the Russell-Bond albedo as a function of wavelength. The large increase with wavelength is the cause of the characteristic red color of the planet. Data from reference 69 indicate that the albedo increases further between $\lambda = 0.70\mu$ and $\lambda = 0.84\mu$ by a factor of 1.4; however, other data have indicated that it does not increase appreciably beyond $\lambda = 0.7\mu$. For design upper limits, one might take into account the previously mentioned factor of 1.56 by raising these curves and flattening them somewhat so as to reduce the variation with wavelength.

The relative variation of total brightness with phase angle is shown in figure 13. Since Mars is not observable from the Earth at phase angles greater than 48°, the curve beyond 48° is merely drawn proportional to the Earth curve. Different curves are indicated for red, green, and blue. As with Venus and the Earth, Mars probably appears bluer at the larger phase angles.

Surface Reflectance

If the sunlit part of a satellite orbit is mainly over the northern hemisphere, the applicable reflectance will be essentially that of the

light regions. Figure 25, from reference 67, gives the observed normal reflectance as a function of wavelength for a typical light area observed at the center of the disk at opposition. Figure 26, based on figure 5 of the same reference but with extensive extrapolation, gives polar diagrams of the light-region reflectance in the plane of incidence, for $\lambda = 0.62\mu$, for several angles of incidence. The general reflectance characteristics seem to be somewhat more Lambertian for the deeper reds. (For a perfect Lambert reflector, the curves of fig. 26 would all be equal superimposed semicircles.)

In the southern hemisphere the dark areas decrease the average reflectance. The decrease is of the order of 15 percent at the red end of the spectrum but is inappreciable at the blue end.

For the blue end of the spectrum the increased scattering from the blue haze and the decreased reflectance from the ground result in appreciably different reflection characteristics. For example, at opposition the disk appears, at least out to 80 percent of the radius from the center, almost uniformly bright in blue light. On the whole, one might suppose the scattering characteristics of the haze to be more or less similar to those of the Earth's dust and haze, but it may be more strongly absorbing.

On the rare occasions when the blue haze seems to disappear, the shapes of the polar reflectance diagrams for blue light seem to approach those of the curves for yellow or red light. The values of the blue reflectance, however, remain very low. At the other extreme, when white or yellow clouds appear, reflectances in general increase and the angular distribution of reflected light becomes less Lambertian. As an illustration of these effects, figure 27 (from ref. 69) shows the relative variation with distance from the center of the disk of the brightness of the light areas, at different wavelengths, for the condition of blue-haze clearing and for two different yellow-fog intensities.

Some allowance for clouds should probably be made in establishing design limits for the reflected radiation under a near-satellite orbit; but the available information is too qualitative and, to some extent, too inconsistent to justify more than arbitrary estimates. In reference 66 are mentioned white clouds as much as 2,000 kilometers long, and photographs are shown of a brilliant opaque yellow cloud that covered the planet between -40° and -55° latitude. Design limits might reasonably be based on such observations, with the white clouds assumed to have 30-percent reflectance across most of the spectrum (see the previous discussion of Earth cloud reflectance), and the yellow clouds assumed to have 30-percent reflectance across all but the blue and violet parts of the spectrum.

Night-Sky Radiation

Mars has two natural satellites, Phobos and Deimos, with diameters of about 16 and 8 kilometers and with orbit radii of 9,370 and 23,500 kilometers, respectively. Their reflection characteristics are assumed to be similar to those of the Moon.

It is not known whether the Martian atmosphere exhibits auroras or has a night glow, or whether Mars has a Lyman-α hydrogen corona. Because of the high altitude (about 25 kilometers) of the haze, there may be a pronounced twilight.

Thermal Radiation

Figure 28 (adapted from ref. 62) shows a radiation scan along an east-west line across the center of the disk, about 1 month after opposition (phase angle of about 20°) and 45° before perihelion. The actual data are for the sunlit part between 0700 hr and 1400 hr (Mars time), and the remainder of the curve is extrapolated and estimated. The maximum temperature occurs about a half hour past noon and is about 30° C; the minimum presumably occurs before sunrise and is generally estimated as between -70° C and -100° C. There are fewer, and less consistent, data for the regions closer to the poles. Observations during the southern midsummer indicated that noon temperatures in the south polar regions could be near 0° C, but that they were probably near -100° C in the north polar regions. Near aphelion, temperatures will be about 10 percent lower than near perihelion.

There is less information concerning temperatures during periods of abnormal weather. Observations during one of the rare clearings (refs. 65 and 70) indicated that the temperature difference between the center of the disk and the east and west limbs was greatly reduced. The dotted curve in figure 28 shows the order of the observed reduction. Observations of a large yellow cloud (ref. 62) indicated a constant temperature of -25° C as it moved across the disk, as if the cloud itself were radiating at the constant temperature of a given altitude in the atmosphere. Possibly at the times when the yellow clouds obscure, or nearly obscure, the surface details, Mars has a substantially uniform radiation temperature of about this value. White clouds appear to be at much higher altitudes - up to 20 kilometers and above - and their thermal-radiation temperatures should then be of the order of -70° C to -80° C, corresponding to the atmospheric temperatures at these altitudes.

The preceding data are based on measurements of the thermal radiation transmitted by the infrared window of the Earth's atmosphere. It

is likely that the spectrum of the Mars radiation is fairly similar to the black-body spectrum; however, the carbon dioxide in the Mars atmosphere should cause a deep dip, between 14μ and 16μ, in the spectrum from the warmer areas, and may cause a peak, in the same wavelength range, in the spectrum from the coldest areas.

In addition to the references already mentioned, reference 71 might be cited as a recent review of the environment of Mars.

Langley Research Center,
National Aeronautics and Space Administration,
Langley Station, Hampton, Va., April 10, 1962.

REFERENCES

1. Ballinger, J. C., Elizalde, J. C., and Christensen, E. H.: Thermal Environment of Interplanetary Space. [Preprint] 344B, Soc. Automotive Eng., 1961.

2. Johnson, Francis.: The Solar Constant. Jour. of Meteorology, vol. 11, no. 6, Dec. 1954, pp. 431-439.

3. Allen, C. W.: Solar Radiation. Quarterly Jour. Roy. Meteorological Soc., vol. 84, no. 362, Oct. 1958, pp. 307-318.

4. Johnson, H. L., and Iriarte, B.: The Sun as a Variable Star. Lowell Observatory Bull. No. 96, vol. IV, no. 8, Mar. 1959, pp. 99-104.

5. Detwiler, C. R., Garrett, D. L., Purcell, J. D., and Tousey, R.: The Intensity Distribution in the Ultraviolet Solar Spectrum. Ann. Géophysique, vol. 17, no. 3, July-Sept. 1961, pp. 9-18.

6. Hinteregger, H. E.: Interplanetary Ionization by Solar Extreme Ultraviolet Radiation. The Astrophysical Jour., vol. 132, no. 3, Nov. 1960, pp. 801-811.

7. Hinteregger, H. E.: Preliminary Data on Solar Extreme Ultraviolet Radiation in the Upper Atmosphere. Jour. Geophys. Res., vol. 66, no. 8, Aug. 1961, pp. 2,367-2,380.

8. Aboud, A., Behring, W. E., and Rense, W. A.: Emission-Line Intensities in the Solar Ultraviolet. The Astrophysical Jour., vol. 130, no. 2, Sept. 1959, pp. 381-383.

9. Violett, T., and Rense, William A.: Solar Emission Lines in the Extreme Ultraviolet. The Astrophysical Jour., vol. 130, no. 3, Nov. 1959, pp. 954-960.

10. Byram, E. T., Chubb, T. A., Friedman, H., Kupperian, J. E., Jr., and Kreplin, R. W.: Intensity of Solar Lyman-Alpha and Adjacent Ultraviolet Emission Lines. The Astrophysical Jour., vol. 128, no. 3, Nov. 1958, pp. 738-740.

11. Friedman, Herbert: The Sun's Ionizing Radiations. Ch. 4 of Physics of the Upper Atmosphere, J. A. Ratcliffe, ed., Academic Press, Inc. (New York), 1960, pp. 133-218.

12. Ditchburn, R. W.: Ultra-Violet Radiation Absorption Cross-Sections. Rocket Exploration of the Upper Atmosphere, R. L. F. Boyd and M. J. Seaton, eds., Pergamon Press Ltd., 1954, pp. 313-326.

13. Allen, C. W.: Astrophysical Quantities. The Athlone Press (London), 1955.

14. Chubb, T. A., Friedman, H., and Kreplin, R. W.: X-Ray Emission Accompanying Solar Flares and Non-Flare Sunspot Maximum Conditions. Space Research, Hilde Kallmann Bijl, ed., Interscience Publ., Inc. (New York), 1960, pp. 695-701.

15. Chubb, T. A., Friedman, H., and Kreplin, R. W.: Measurements Made of High-Energy X-Rays Accompanying Three Class 2+ Solar Flares. Jour. Geophys. Res., vol. 65, no. 6, June 1960, pp. 1,831-1,832.

16. Peterson, L. E., and Winckler, J. R.: Gamma-Ray Burst From a Solar Flare. Jour. Geophys. Res., vol. 64, no. 7, July 1959, pp. 697-707.

17. Coulson, Kinsell L.: The Flux of Radiation From the Top of a Rayleigh Atmosphere. Sci. Rep. No. 1 (AFCRC TN 59 402, ASTIA AD 216 317), Dept. Meteorology, Univ. of California at Los Angeles, Jan. 1959.

18. Coulson, K. L., and Furukawa, P. M.: Distributions of Atmospheric Radiative Heating and Cooling. Sci. Rep. 2 (AFCRL-TN-60-835), Stanford Res. Inst. (Menlo Park, Calif.), Nov. 1960.

19. Toolin, Robert B., and Stakutis, Vincent J.: Qualitative Indication of Nadir Sky Blue. Jour. Optical Soc. of America (Letters to the Editor), vol. 48, no. 1, Jan. 1958, pp. 71-72.

20. Duntley, Seibert Q., Boileau, Almerian, Gordon, Jacqueline, and Harris, James L.: Maps of Sky Luminance at Various Altitudes. SIO Ref. 60-12, Visibility Lab., Univ. of California, Feb. 1960. (Available from ASTIA as AD 240679.)

21. Van de Hulst, H. C.: Scattering in the Atmospheres of the Earth and the Planets. The Atmospheres of the Earth and Planets, Second ed., Gerard P. Kuiper, ed., The Univ. of Chicago Press, c.1952, pp. 49-111

22. London, Julius: A Study of the Atmospheric Heat Balance. AFCRC-TR-57-287, ASTIA no. 117227, College Eng., New York Univ., July 1957.

23. Anon.: Handbook of Geophysics. Revised ed., The Macmillan Co., 1961.

24. Hewson, E. W.: The Reflection, Absorption, and Transmission of Solar Radiation by Fog and Cloud. Quarterly Jour. Roy. Meteorological Soc. vol. 69, no. 298, 1943, pp. 47-62.

25. Kuiper, Gerard P.: Planetary Atmospheres and Their Origin. The Atmospheres of the Earth and Planets, Second ed., Gerard P. Kuiper, ed., The Univ. of Chicago Press, c.1952, pp. 306-405.

26. Krinov, E. L. (G. Belkov, trans.): Spectral Reflectance Properties of Natural Formations. Tech. Translation TT-439, Nat. Res. Council of Canada (Ottawa), 1953.

27. Burt, Wayne V.: Albedo Over Wind-Roughened Water. Jour. Meteorology, vol. II, no. 4, Aug. 1954, pp. 283-290.

28. Anderson, Ernest R.: Energy-Budget Studies. Geological Survey Cir. No. 229, U.S. Dept. Interior, 1952, pp. 71-119.

29. Cox, Charles, and Munk, Walter: The Measurement of the Roughness of the Sea Surface From Photographs of the Sun's Glitter - Part I: The Method. SIO Ref. 52-61 (AF Tech. Rep. No. 2), Univ. California, Nov. 24, 1952.

30. Fritz, S., and Wexler, H.: Planet Earth as Seen From Space. Planets and Satellites, Gerard P. Kuiper and Barbara M. Middlehurst, eds., The Univ. of Chicago Press, c.1961, pp. 1-11.

31. Fritz, Sigmund: The Albedo of the Planet Earth and of Clouds. Jour. Meteorology, vol. 6, no. 4, Aug. 1949, pp. 277-282.

32. Houghton, Henry G.: On the Annual Heat Balance of the Northern Hemisphere. Jour. Meteorology, vol. 11, no. 1, Feb. 1954, pp. 1-9.

33. Danjon, André: Albedo, Color, and Polarization of the Earth. The Earth as a Planet, Gerard P. Kuiper, ed., The Univ. of Chicago Press, c.1954, pp. 726-738.

34. Wexler, Raymond: Satellite Observations of Infrared Radiation. First Semi-Annual Tech. Summary Rep. (Contract No. AF 19(604)-5968), Air Force Cambridge Res. Center, Dec. 24, 1959.

35. Wexler, Raymond: Satellite Observations of Infared Radiation. GRD-TN-60-493, Air Force Res. Div. (Bedford, Mass.), June 30, 1960.

36. Hales, J. Vern, and Zdunkowski, Wilford G.: The Long Wave Flux Density Leaving the Earth Under Various Meteorological Conditions. Sci. Rep. No. 1 (AFCRC-TN-59-212, ASTIA Doc. No. AD212552), Intermountain Weather, Inc. (Salt Lake City, Utah), Jan. 1959.

37. Suomi, V. E.: The Thermal Radiation Balance Experiment on Board Explorer VII. Juno II Summary Project Report. Vol. I - Explorer VII Satellite. NASA TN D-608, 1961, pp. 273-305.

38. Weinstein, Melvin, and Suomi, Verner E.: Analysis of Satellite Infrared Radiation Measurements on a Synoptic Scale. Monthly Weather Rev., vol. 89, no. 11, Nov. 1961, pp. 419-428.

39. Staffs of Aeronomy and Meteorology Div. and Meteorological Satellite Lab.: Tiros II - Radiation Data Catalog. Vol. I. Goddard Space Flight Center, Aug. 15, 1961.

40. Roach, F. E., Pettit, Helen B., Tandberg-Hanssen, E., and Davis, Dorothy N.: Observations of the Zodiacal Light. The Astrophysical Jour., vol. 119, no. 1, Jan. 1954, pp. 253-273.

41. Megill, Lawrence R., and Roach, Franklin E.: The Integrated Starlight Over the Sky. NBS Tech. Note 106, U.S. Dept. Commerce, June 1961.

42. Bates, D. R.: The Airglow. Ch. 5 of Physics of the Upper Atmosphere, J. A. Ratcliffe, ed., Academic Press, Inc. (New York), 1960, pp. 219-267.

43. Störmer, Carl: The Polar Aurora. The Clarendon Press (Oxford), 1955.

44. Ingham, M. F.: Observations of the Zodiacal Light From a Very High Altitude Station - IV. The Nature and Distribution of the Interplanetary Dust. Monthly Notices, Roy. Astronomical Soc., vol. 122, no. 2, 1961, pp. 157-176.

45. Divari, N. B., and Asaad, A. S.: Photoelectric Observations of the Zodiacal Light in Egypt. Soviet Astronomy - AJ, vol. 3, no. 5, Mar.-Apr. 1960, pp. 832-838.

46. Martynov, D. Ya.: The Visual Stellar Magnitude of the Sun, the Moon, and the Lux. Soviet Astronomy - AJ, vol. 3, no. 4, Jan.-Feb. 1960, pp. 633-644.

47. Stair, Ralph, and Johnson, Russell: Ultraviolet Spectral Radiant Energy Reflected From the Moon. Res. Paper 2434, Jour. Res. Nat. Bur. Standards, vol. 51, no. 2, Aug. 1953, pp. 81-84.

48. Rougier, G.: Photométrie photoélectrique de la lune. Chapitre IV - Réduction des observations. Ann. l'Observatoire Strasbourg, Vol. 2, Fasc. 3, 1933, pp. 255-292.

49. Bruner, Elmo C., Jr.: Photometric Observations of the Lunar Eclipse of November 17-18, 1956. Pub. Astronomical Soc. Pacific, vol. 69, no. 410, Oct. 1957, pp. 431-435.

50. Orlova, N. S.: Selected Articles on Light Scattering and Photometric Relief of the Lunar Surface. NASA TT F-75, 1962.

51. Minnaert, M.: The Reciprocity Principle in Lunar Photometry. The Astrophysical Jour., vol. 93, no. 3, May 1941, pp. 403-410.

52. Russell, Henry Norris: On the Albedo of the Planets and Their Satellites. The Astrophysical Jour., vol. XLIII, no. 3, Apr. 1916, pp. 173-196.

53. Struve, Otto: Photometry of the Moon. Sky and Telescope, vol. XX, no. 2, Aug. 1960, pp. 70-73.

54. Geoffrion, Ann R., Korner, Marjorie, and Sinton, William M.: Isothermal Contours of the Moon. Lowell Observatory Bull. No. 106, vol. V, no. 1, May 27, 1960, pp. 1-15.

55. Pettit, Edison, and Nicholson, Seth B.: Lunar Radiation and Temperatures. Contributions From the Mt. Wilson Observatory, No. 392, Carnegie Inst. of Washington (reprinted from The Astrophysical Jour., vol. LXXI, 1930, pp. 102-135).

56. Giraud, Alain: A Study of Lunar Thermal Emission. Rep. No. 03544-1-T, College Eng., Univ. of Michigan, Sept. 1960.

57. Pettit, Edison: Radiation Measurements on the Eclipsed Moon. The Astrophysical Jour., vol. 91, no. 4, 1940, pp. 408-420.

58. Bobrovnikoff, N. T.: Natural Environment of the Moon. WADC Phase Tech. Note 3, U.S. Air Force, June 1959.

59. De Vaucouleurs, G.: Phase Curves and Albedos of Terrestrial Planets. GCA Tech. Rep. 61-26-A (Contract No. AF 33(616)-7413), Geophysics Corp. of America (Bedford, Mass.), June 1961. (Available from ASTIA as AD 261 165.)

60. Kozyrev, N. A.: Molecular Absorption in the Violet Region of the Spectrum of Venus. Publ. Crimean Astroph. Observ., vol. 12, 1954, pp. 177-181.

61. Heyden, F. J., Kiess, C. C., and Kiess, Harriet K.: Spectrum of Venus in the Violet and Near-Ultraviolet. Science, vol. 130, no. 3383, Oct. 30, 1959, p. 1195.

62. Sinton, William M., and Strong, John: Observations of the Infrared Emission of Planets and Determination of Their Temperatures. Contract Nonr 248(01), Lab. of Astrophys. and Phys. Meteorology, The Johns Hopkins Univ., Apr. 15, 1960. (Available from ASTIA as AD 250440.)

63. Shaw, John H., and Bobrovnikoff, N. T.: Natural Environment of the Planet Venus. WADC Phase Tech. Note 2, U.S. Air Force, Feb. 1959.

64. Asbrook, Joseph: The New IAU Nomenclature for Mars. Sky and Telescope, vol. XVIII, no. 1, Nov. 1958, pp. 23-25.

65. De Vaucouleurs, Gerard: Physics of the Planet Mars. Faber and Faber, Ltd. (London), 1954.

66. Dollfus, A.: Visual and Photographic Studies of Planets at the Pic du Midi. Planets and Satellites, Gerard P. Kuiper and Barbara M. Middlehurst, eds., The Univ. of Chicago Press, c.1961, pp. 534-571.

67. Dollfus, Audoin: Propriétés photométriques des contrées désertiques sur la planète Mars. Comptes Rendus, t. 244, no. 2, Jan 7, 1957, pp. 162-164.

68. De Vaucouleurs, G.: Multicolor Photometry of Mars in 1958. Planetary and Space Sci., vol. 2, no. 1, Oct. 1959, pp. 26-32.

69. Barabashov, N. P., and Garazha, V. I.: Some Remarks on the Dust and Haze Formations on Mars. Soviet Astronomy - AJ, vol. 4, no. 3, Nov.-Dec. 1960, pp. 473-479.

70. Coblentz, W. W., Lampland, C. O., and Menzel, D. H.: Temperatures of Mars, 1926, as Derived From Water-Cell Transmissions. Pub. Astronomical Soc. Pacific, vol. 39, no. 228, 1927, pp. 97-100.

71. Shaw, J. H.: Natural Environment of the Planet Mars. WADC Phase Tech. Note 1, U.S. Air Force, Feb. 1959.

TABLE I.- SOLAR SPECTRAL IRRADIANCE OUTSIDE THE ATMOSPHERE[a]

[λ = Wavelength; H_λ = Spectral intensity; P_λ = Percent of total energy < λ]

λ, A	H_λ, $\frac{\text{watts}}{m^2\text{-A}}$	P_λ, %	λ, A	H_λ, $\frac{\text{watts}}{m^2\text{-A}}$	P_λ, %	λ, A	H_λ, $\frac{\text{watts}}{m^2\text{-A}}$	P_λ, %	λ, A	H_λ, $\frac{\text{watts}}{m^2\text{-A}}$	P_λ, %	λ, A	H_λ, $\frac{\text{watts}}{m^2\text{-A}}$	P_λ, %
2,200	0.0030	0.02	3,600	0.116	5.47	5,000	0.198	23.5	6,800	0.151	46.7	26,000	0.00445	96.90
2,250	.0042	.03	3,650	.129	5.89	5,050	.197	24.2	6,900	.148	47.8	27,000	.00390	97.21
2,300	.0052	.05	3,700	.133	6.36	5,100	.196	24.9	7,000	.144	48.8	28,000	.00343	97.47
2,350	.0054	.07	3,750	.132	6.84	5,150	.189	25.6	7,100	.141	49.8	29,000	.00303	97.72
2,400	.0058	.09	3,800	.123	7.29	5,200	.187	26.3	7,200	.137	50.8	30,000	.00268	97.90
2,450	.0064	.11	3,850	.115	7.72	5,250	.192	26.9	7,300	.134	51.8	31,000	.00230	98.08
2,500	.0064	.13	3,900	.112	8.13	5,300	.195	27.6	7,400	.130	52.7	32,000	.00214	98.24
2,550	.010	.16	3,950	.120	8.54	5,350	.197	28.3	7,500	.127	53.7	33,000	.00191	98.39
2,600	.013	.20	4,000	.154	9.03	5,400	.198	29.0	8,000	.1127	57.9	34,000	.00171	98.52
2,650	.020	.27	4,050	.188	9.65	5,450	.198	29.8	8,500	.1003	61.7	35,000	.00153	98.63
2,700	.025	.34	4,100	.194	10.3	5,500	.195	30.5	9,000	.0895	65.1	36,000	.00139	98.74
2,750	.022	.43	4,150	.192	11.0	5,550	.192	31.2	9,500	.0803	68.1	37,000	.00125	98.83
2,800	.024	.51	4,200	.192	11.7	5,600	.190	31.8	10,000	.0725	70.9	38,000	.00114	98.91
2,850	.034	.62	4,250	.189	12.4	5,650	.189	32.5	11,000	.0606	75.7	39,000	.00103	98.99
2,900	.052	.77	4,300	.178	13.0	5,700	.187	33.2	12,000	.0501	79.6	40,000	.00095	99.05
2,950	.063	.98	4,350	.182	13.7	5,750	.187	33.9	13,000	.0406	82.9	41,000	.00087	99.13
3,000	.061	1.23	4,400	.203	14.4	5,800	.187	34.5	14,000	.0328	85.5	42,000	.00080	99.18
3,050	.067	1.43	4,450	.215	15.1	5,850	.185	35.2	15,000	.0267	87.6	43,000	.00073	99.23
3,100	.076	1.69	4,500	.220	15.9	5,900	.184	35.9	16,000	.0220	89.4	44,000	.00067	99.29
3,150	.082	1.97	4,550	.219	16.7	5,950	.183	36.5	17,000	.0182	90.83	45,000	.00061	99.33
3,200	.085	2.26	4,600	.216	17.5	6,000	.181	37.2	18,000	.0152	92.03	46,000	.00056	99.38
3,250	.102	2.60	4,650	.215	18.2	6,100	.177	38.4	19,000	.01274	93.02	47,000	.00051	99.41
3,300	.115	3.02	4,700	.217	19.0	6,200	.174	39.7	20,000	.01079	93.87	48,000	.00048	99.45
3,350	.111	3.40	4,750	.220	19.8	6,300	.170	40.9	21,000	.00917	94.58	49,000	.00044	99.48
3,400	.111	3.80	4,800	.216	20.6	6,400	.166	42.1	22,000	.00785	95.20	50,000	.00042	99.51
3,450	.117	4.21	4,850	.203	21.3	6,500	.162	43.3	23,000	.00676	95.71	60,000	.00021	99.74
3,500	.118	4.63	4,900	.199	22.0	6,600	.159	44.5	24,000	.00585	96.18	70,000	.00012	99.86
3,550	.116	5.04	4,950	.204	22.8	6,700	.155	45.6	25,000	.00509	96.57	100,000	.000023	99.97

[a]Data from reference 2.

TABLE II.- ENERGY DISTRIBUTION IN THE FAR ULTRAVIOLET PORTION OF THE SOLAR SPECTRUM

Wavelength band or wavelength, λ_1-λ_2 or λ, A	Photon flux density, photons-cm^{-2}-sec^{-1}	Energy flux density, erg-cm^{-2}-sec^{-1}
From reference 6[a]		
1,216	370×10^9	6.0
[b]1,300-1,040	50	.85
1,040-1,000	45	.90
1,000-950	40	.80
950-912	20	.40
912-850	50	1.10
850-650	30	.80
650-475	30	1.10
[c]475-300	10	.50
304	6	.40
300-250	7	.50
250-170	8	.76
170-110	3	.45
110-60	2	.46
1,300-60	670×10^9	15
From reference 7		
1,216	200×10^9	3.3
[b]1,300-1,200	10	.2
1,200-1,100	7	.1
1,100-1,000	8	.13
1,000-911	8	.16
911-800	9	.20
800-700	1.4-3	.04-.10
700-500	7.8	.26
500-400	1.5	.07
304	4	.25
[c]400-260	3.7	.22
260-166	6.5	.65
166-105	.5	.07
105-60	1.5	.35
1,300-60	270×10^9	6

[b]Excluding H Ly-α.

[c]Excluding He^+ Ly-α.

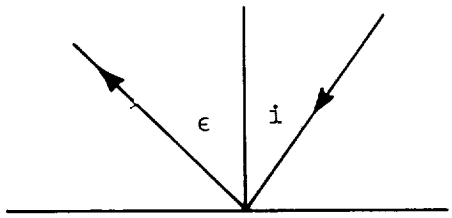

TABLE III.- REFLECTANCE OF LUNAR MARIA; REFLECTED RAY IN THE PLANE OF INCIDENCE[a]

ϵ, deg \ i, deg	0	10	20	30	40	50	60	70
-80	0.024	0.034	0.032	0.034	0.039	0.049	-----	-----
-70	.026	.034	.036	.039	.047	.063	0.111	0.237
-60	.027	.035	.040	.046	.057	.086	.162	.128
-50	.030	.038	.044	.058	.074	.126	.106	.081
-40	.034	.042	.053	.075	.106	.089	.069	.057
-30	.040	.050	.065	.094	.076	.062	.052	.043
-20	.049	.063	.086	.071	.058	.048	.039	.035
-10	.066	.082	.065	.053	.044	.040	.032	.030
0	.081	.070	.051	.040	.036	.033	.026	.025
10	0.066	0.053	0.042	0.033	0.030	0.028	0.022	0.021
20	.049	.042	.035	.029	.027	.024	.019	.019
30	.040	.034	.031	.026	.024	.020	.018	.017
40	.034	.030	.027	.025	.023	.017	.017	.016
50	.030	.028	.025	.023	.020	.016	.016	.015
60	.027	.026	.023	.021	.018	.015	.014	.014
70	.026	.024	.023	.020	.016	.013	-----	-----
80	.024	-----	-----	-----	-----	-----	-----	-----

[a]Data from reference 50.

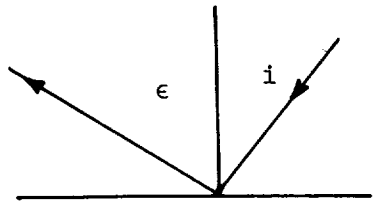

TABLE IV.- REFLECTANCE OF LUNAR CONTINENTS; REFLECTED RAY IN THE PLANE OF INCIDENCE[a]

ϵ, deg \ i, deg	0	10	20	30	40	50	60	70
-80	0.028	-----	0.045	0.062	0.075	0.102	-----	-----
-70	.036	0.043	.051	.074	.087	.120	0.190	0.362
-60	.043	.052	.058	.087	.100	.150	.248	.243
-50	.051	.062	.067	.103	.124	.193	.171	.156
-40	.061	.072	.081	.124	.161	.144	.117	.112
-30	.072	.087	.109	.143	.124	.100	.090	.089
-20	.086	.104	.131	.120	.092	.079	.072	.073
-10	.102	.126	.110	.098	.074	.065	.058	.061
0	.124	.108	.088	.078	.061	.052	.047	.050
10	0.102	0.084	0.072	0.064	0.053	0.045	0.040	0.045
20	.086	.073	.062	.053	.046	.037	.034	.038
30	.072	.060	.053	.042	.037	.032	.030	.035
40	.061	.052	.047	.035	.031	.027	.027	.032
50	.051	.042	.037	.030	.027	.025	.026	.030
60	.043	.035	.032	.025	.024	.025	.025	.027
70	.036	.025	.025	.022	.022	.025	.025	.027
80	.028	.017	.017	.020	.020	.025	.025	.027

[a]Data from reference 50.

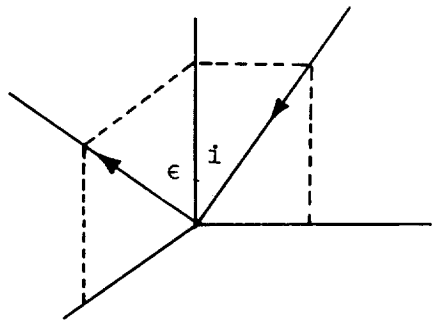

TABLE V.- REFLECTANCE OF LUNAR MARIA; REFLECTED RAY IN PLANE NORMAL TO PLANE OF INCIDENCE

ϵ, deg \ i, deg	10	20	30	40	50	60	70	80
10	0.062	0.050	0.039	0.035	0.032	0.027	0.026	0.024
20	.050	.046	.038	.034	.032	.028	.026	.026
30	.039	.038	.037	.033	.032	.030	.027	.028
40	.035	.034	.033	.033	.032	.032	.027	.031
50	.032	.032	.032	.032	.033	.033	.032	.035
60	.027	.028	.030	.032	.033	.038	.038	.042
70	.026	.026	.027	.027	.032	.038	.047	.054
80	.024	.026	.028	.031	.035	.042	.054	.080

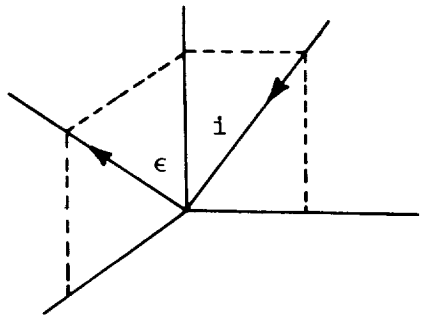

TABLE VI.- REFLECTANCE OF LUNAR CONTINENTS; REFLECTED RAY IN PLANE NORMAL TO PLANE OF INCIDENCE

ϵ, deg \ i, deg	10	20	30	40	50	60	70	80
10	0.095	0.084	0.074	0.061	0.052	0.045	0.043	0.029
20	.084	.076	.070	.061	.052	.046	.044	.030
30	.074	.070	.066	.060	.054	.046	.045	.032
40	.061	.061	.060	.056	.055	.048	.046	.037
50	.052	.052	.054	.055	.050	.051	.050	.047
60	.045	.046	.046	.048	.051	.052	.055	.064
70	.043	.044	.045	.046	.050	.055	.065	.082
80	.029	.030	.032	.037	.047	.064	.082	.114

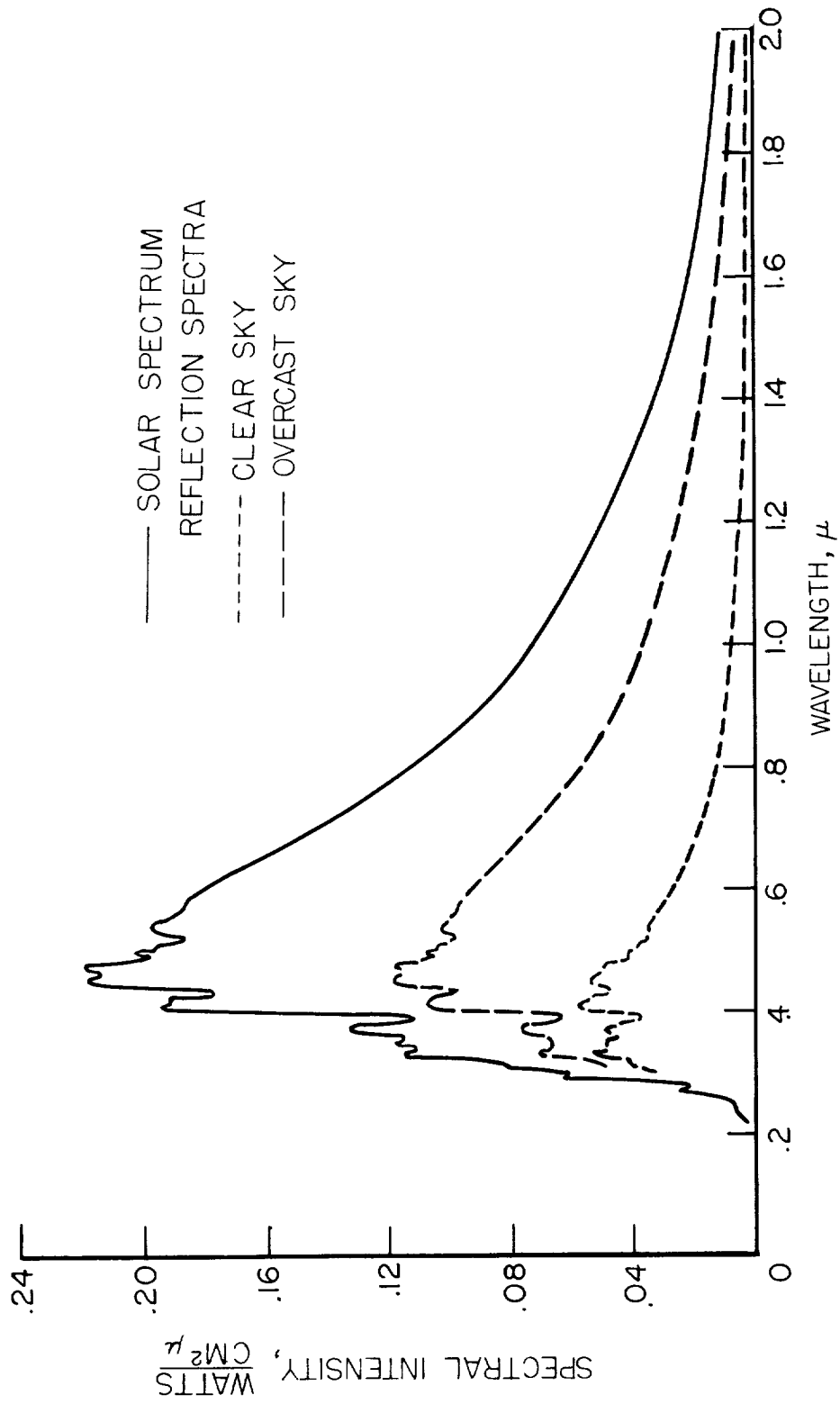

Figure 1.- Solar spectrum compared with theoretical Earth-reflection spectra for diffusely reflecting gray surfaces under a Rayleigh atmosphere. The reflection spectra are for solar zenith angles of 60°. The clear-sky reflection spectrum is for a ground reflectance of 0.1; the overcast-sky reflection spectrum is for a cloud reflectance of 0.5, with cloud top at an altitude of 11,000 feet.

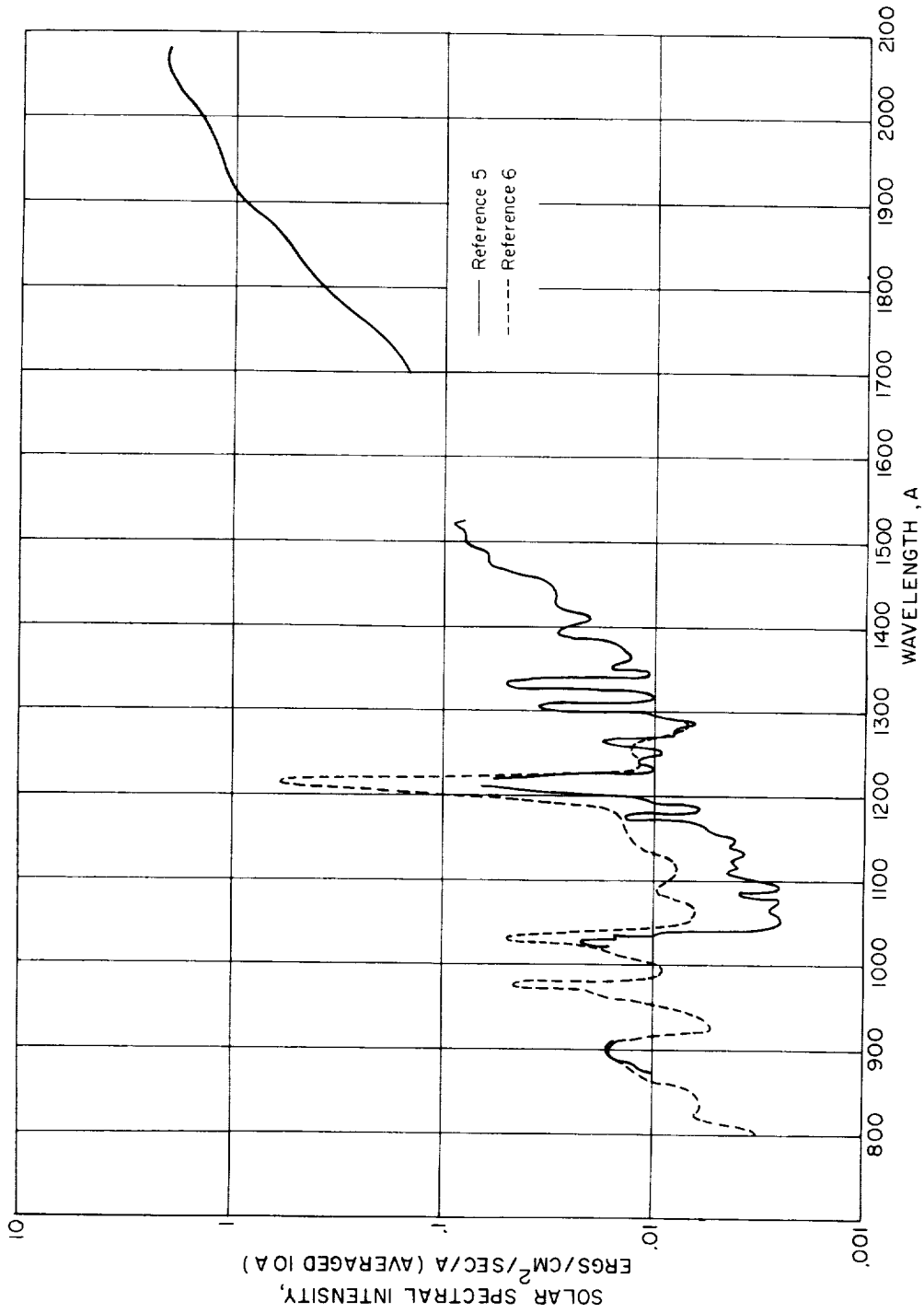

(a) 800 A to 2,100 A.

Figure 2.- Ultraviolet solar spectrum.

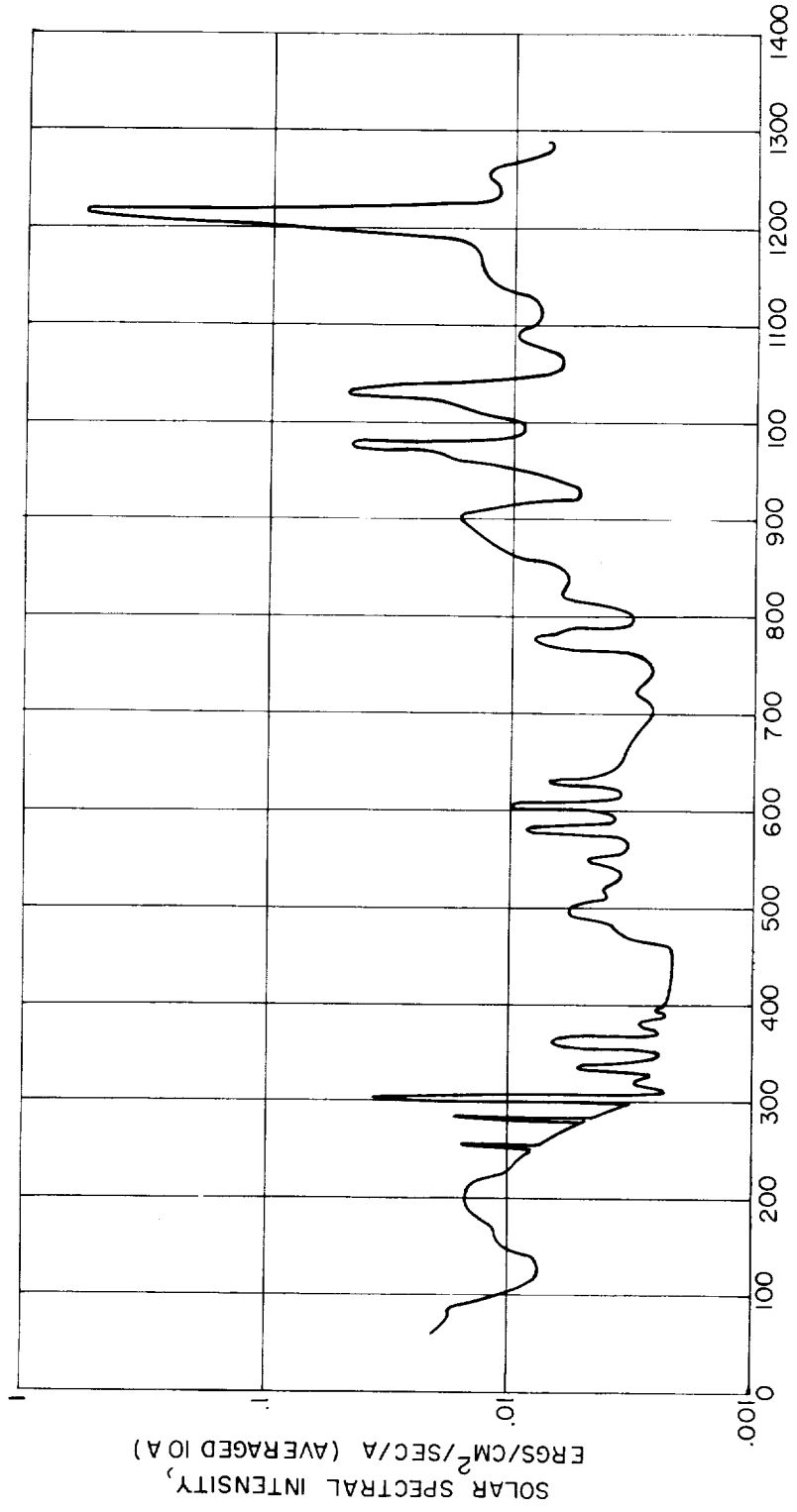

(b) 60 A to 1,300 A (ref. 6, copyright 1960 by the University of Chicago).

Figure 2.- Concluded.

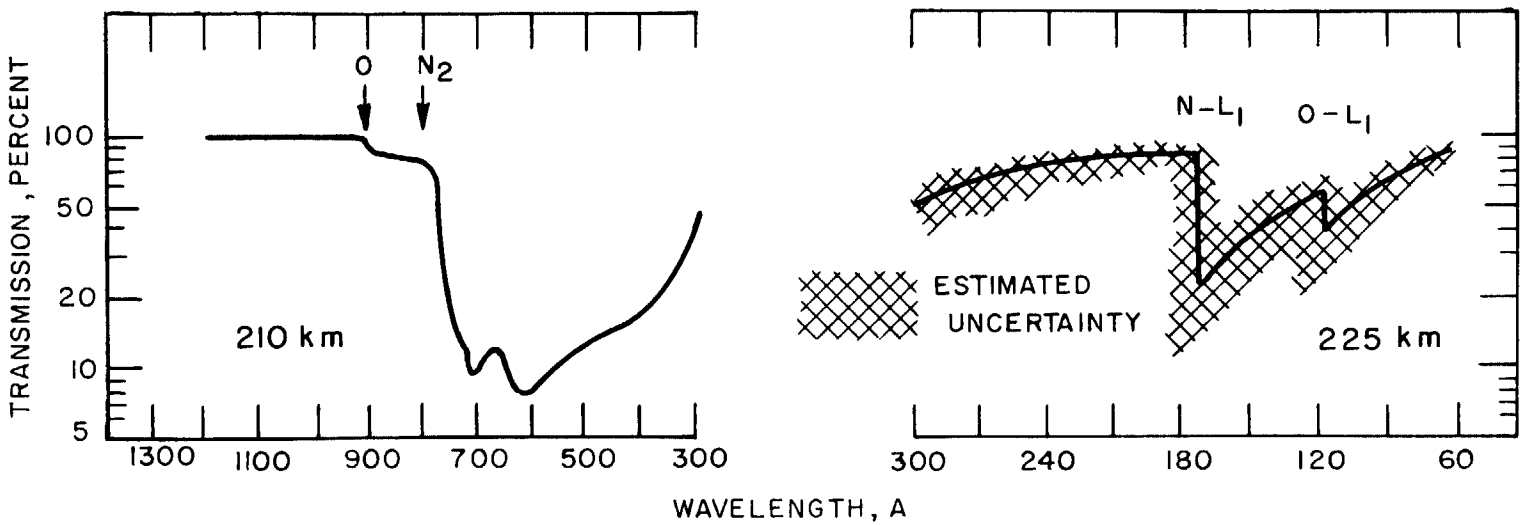

Figure 3.- Atmospheric transmissions used in reference 6 (copyright 1960 by the University of Chicago) for correcting intensities measured at the indicated altitudes. Residual atmosphere assumed to consist of equal numbers of O and N_2 molecules. The curve on the left corresponds to an absorbing column of 1.35×10^{17} particles per sq cm; the curve on the right, to 1.0×10^{17} particles per sq cm. These values include the correction for the secant of the solar zenith angle (60°). The locations of the L_1 absorption limits of O and N are indicated in the right-hand figure.

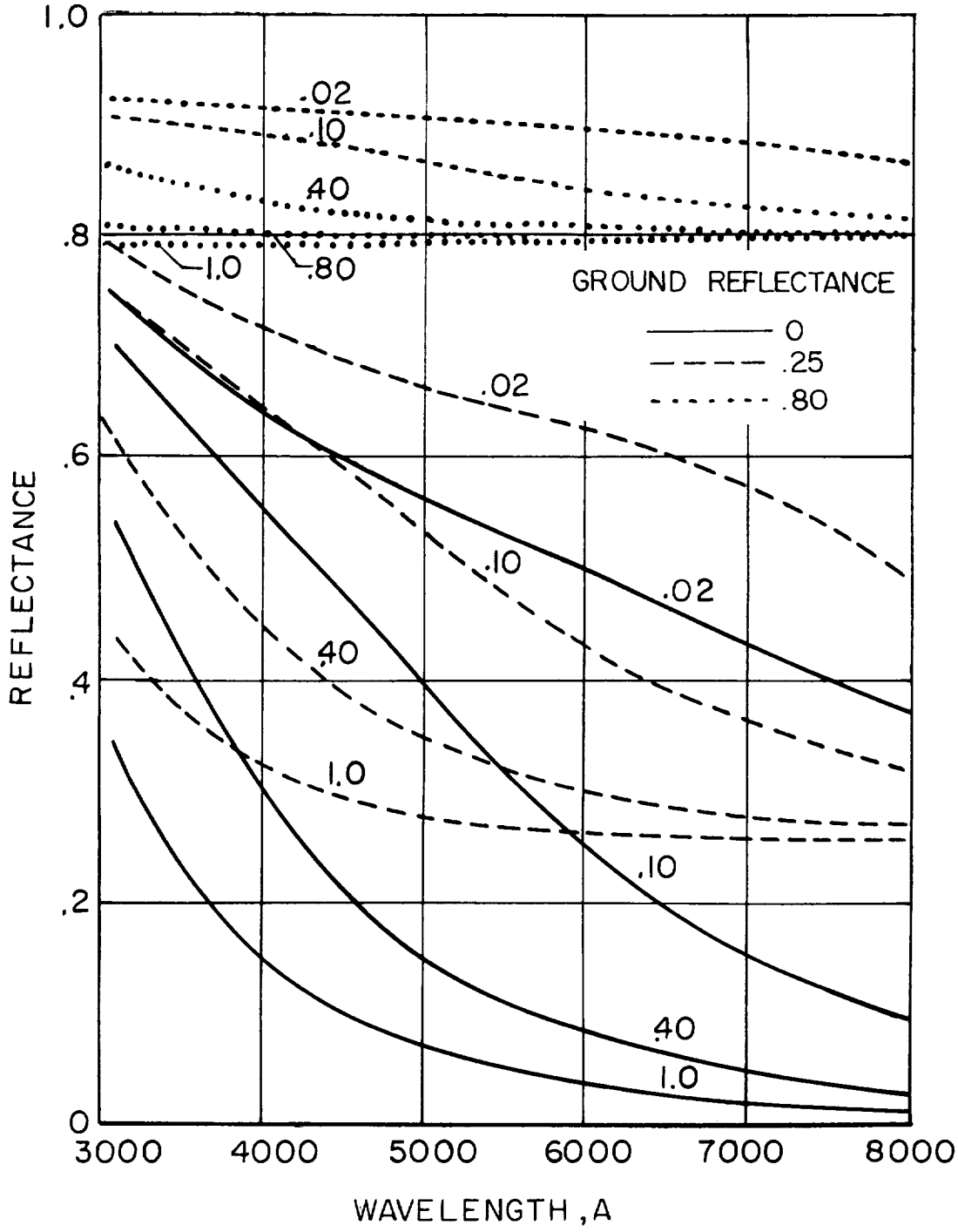

Figure 4.- Theoretical reflectance of Rayleigh atmosphere with underlying ground. The numbers on the curves are the sines of the Sun elevation angles.

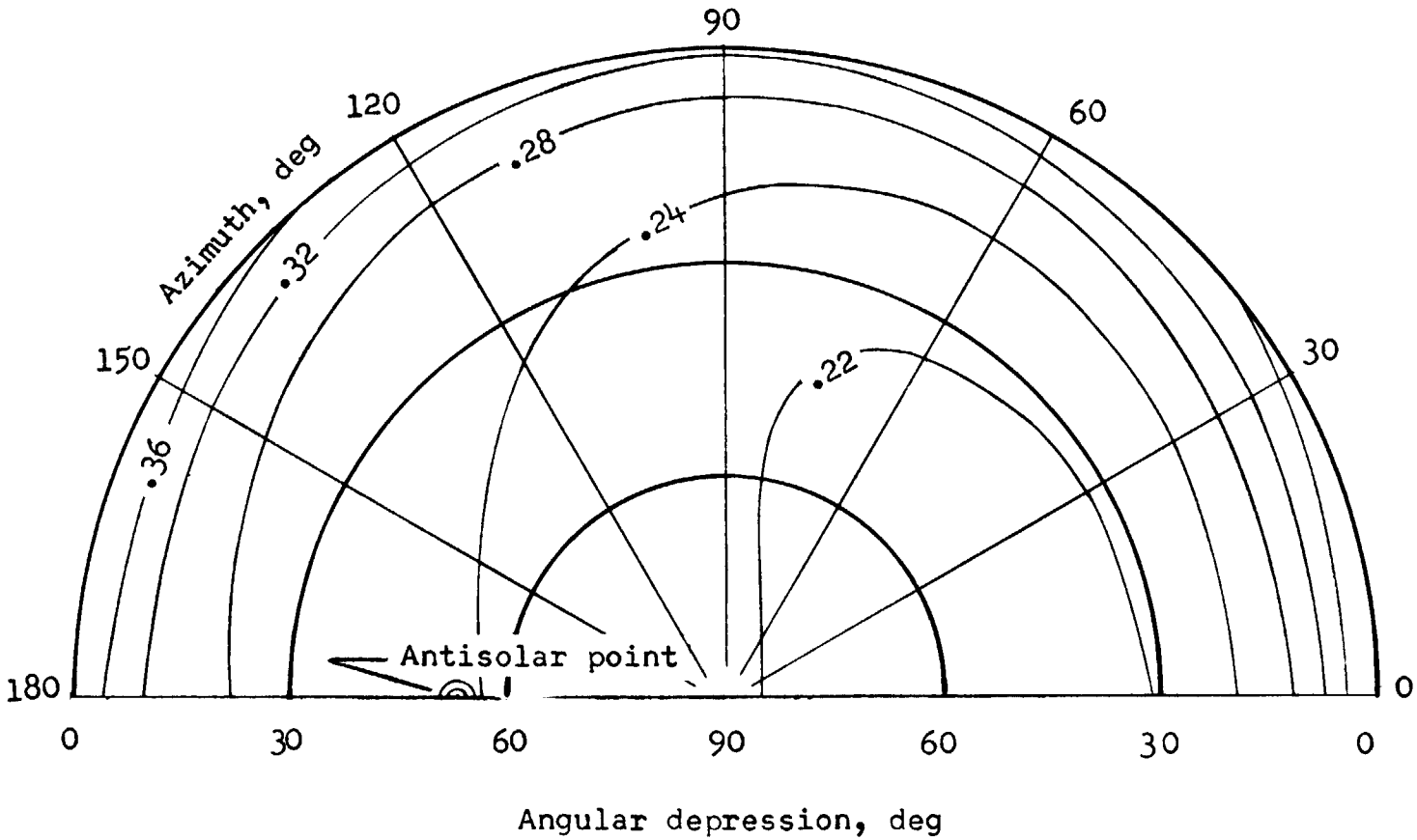

Figure 5.- Calculated distribution of relative intensity of reflected radiation from the lower hemisphere, for λ = 4,950 A, ground reflectance (diffuse) of 0.25, and Sun elevation angle of 53° (from ref. 17).

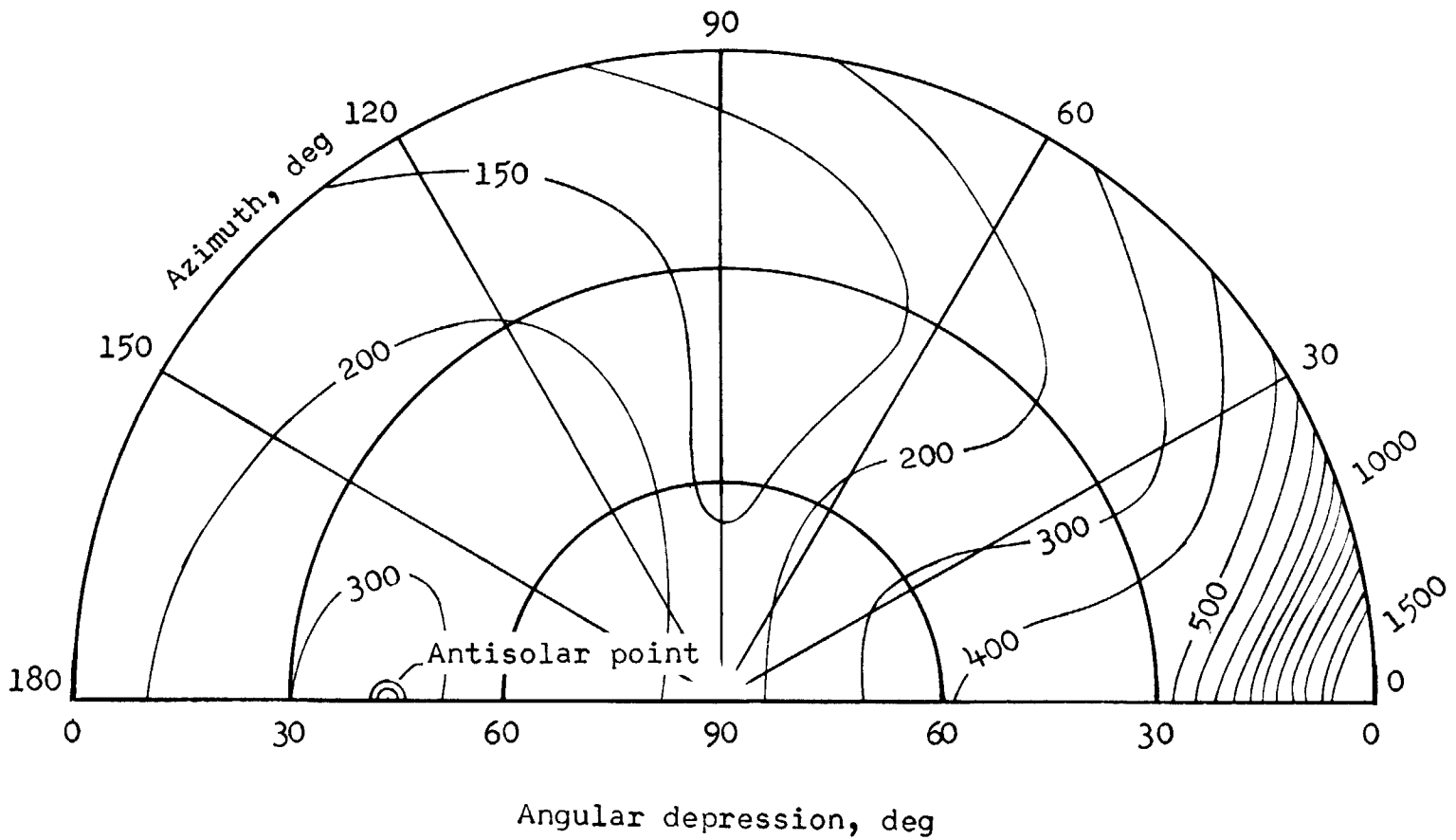

(a) Isoluminance plots of the lower hemisphere, as observed from an altitude of 98,000 feet, above a relatively turbid atmosphere (by V. J. Stakutis, given in ref. 17). Luminance is in candles/sq ft. For comparison, the luminance of a white Lambert surface normal to the Sun's rays outside the atmosphere is 4,200 candles/sq ft.

Figure 6.- Experimental observations of reflected solar radiation for comparison with figure 5.

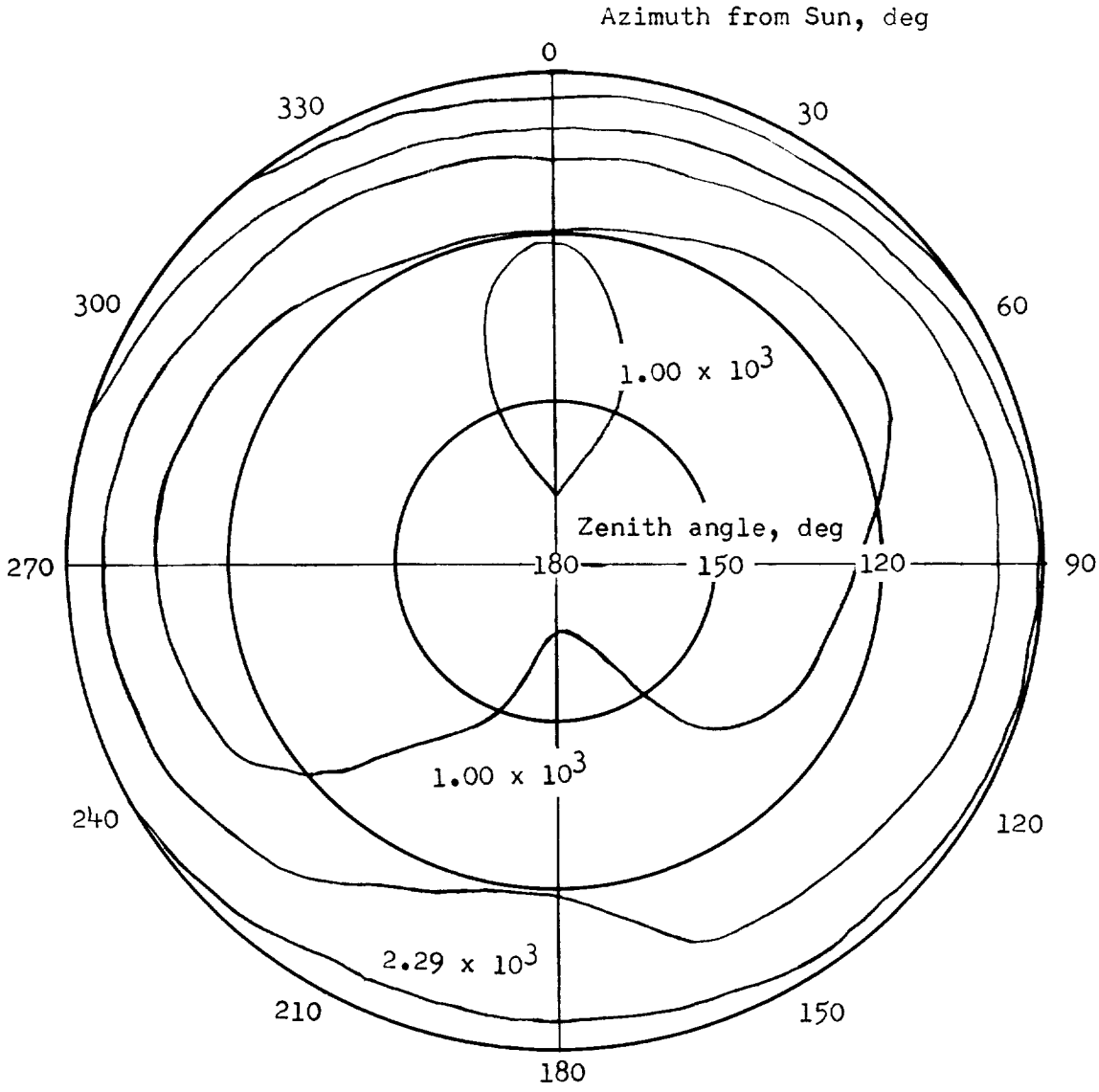

(b) Isoluminance plots of the lower hemisphere as observed from an altitude of 20,000 feet, with the Sun at 24^{o} elevation. The day was described as "clear with scattered clouds between 16,000 and 17,000 feet altitude." Luminance is in foot-lamberts. For comparison, the luminance of a white Lambert surface normal to the Sun's rays outside the atmosphere is 13.2×10^{3} foot-lamberts.

Figure 6.- Concluded.

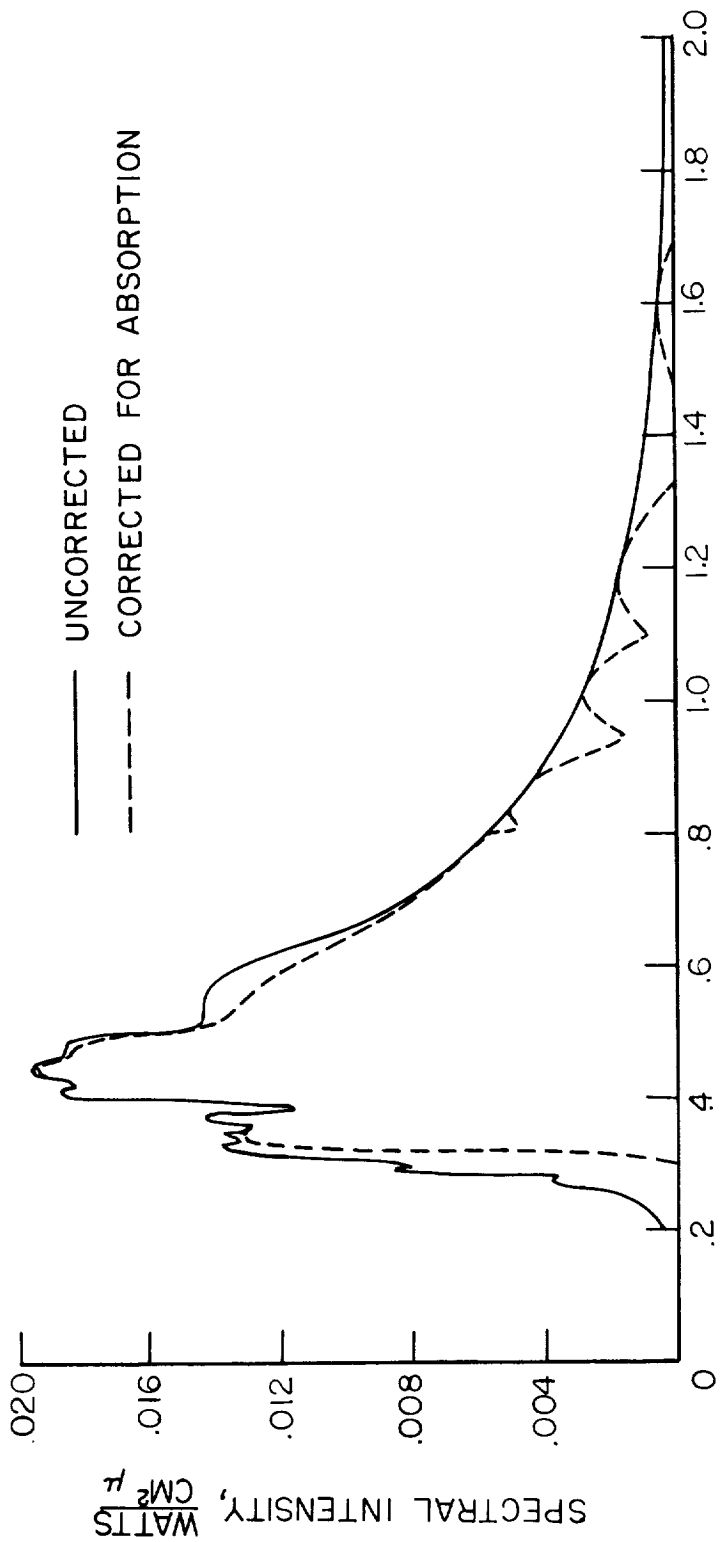

Figure 7.- Spectrum of sunlight scattered out of the atmosphere by dust and water vapor. Sun at 30° elevation angle; 2 centimeters of precipitable water in the atmosphere. Dashed curve includes correction for atmospheric absorption.

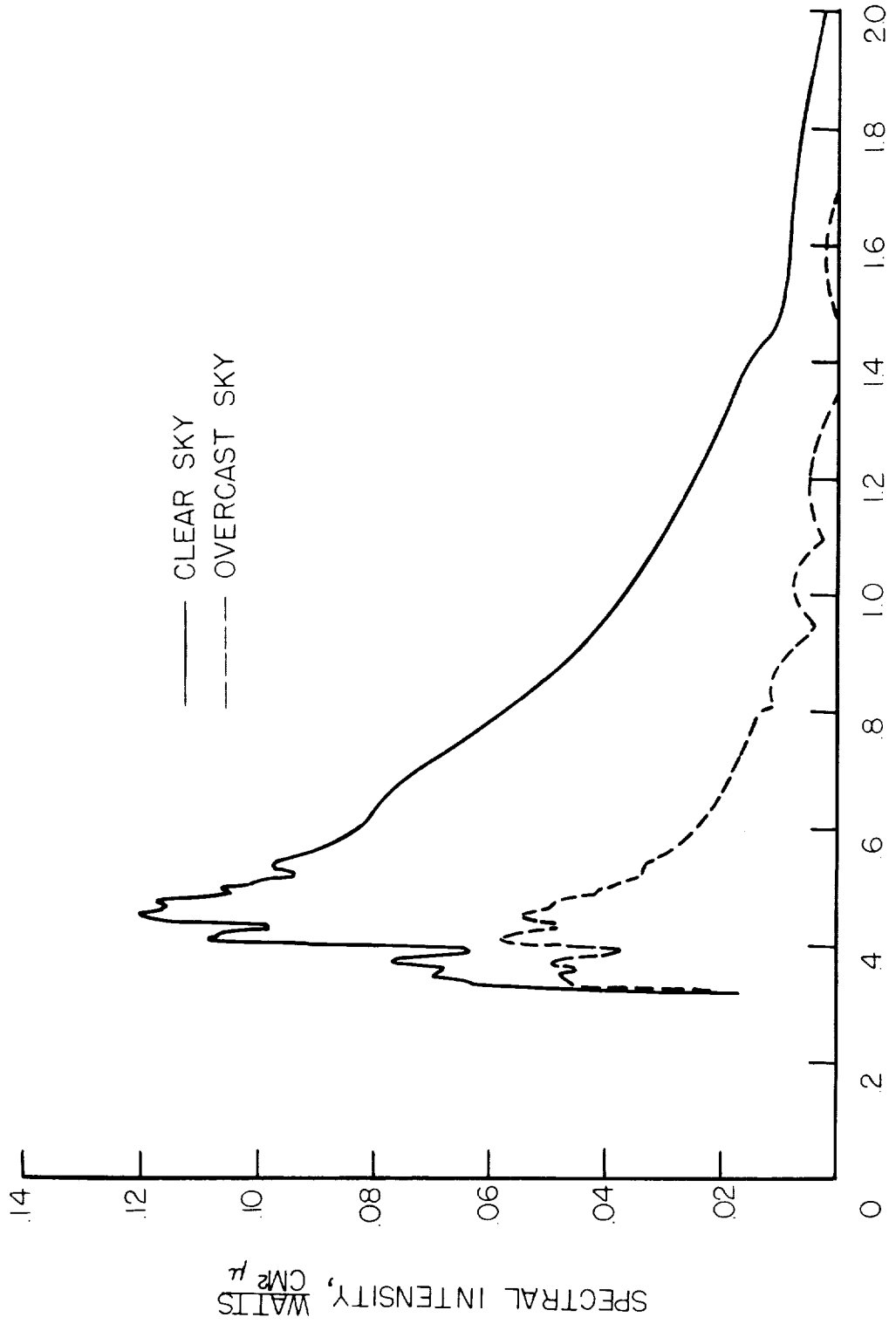

Figure 8.- Reflection spectra of figure 1 corrected for atmospheric absorption.

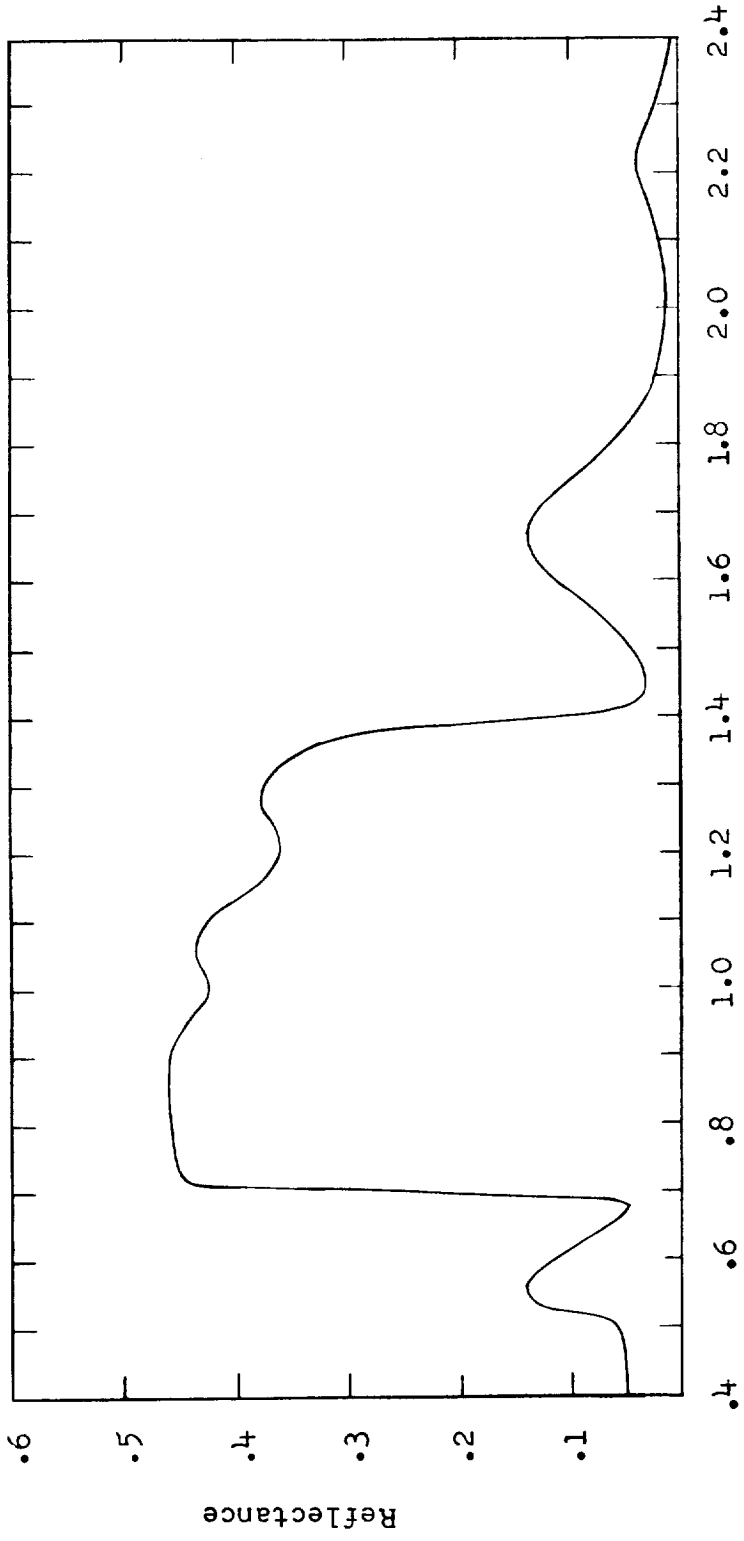

Figure 9.- Schematic spectral reflectance of the higher chlorophyll-containing plants (from ref. 25, copyright 1952 by the University of Chicago).

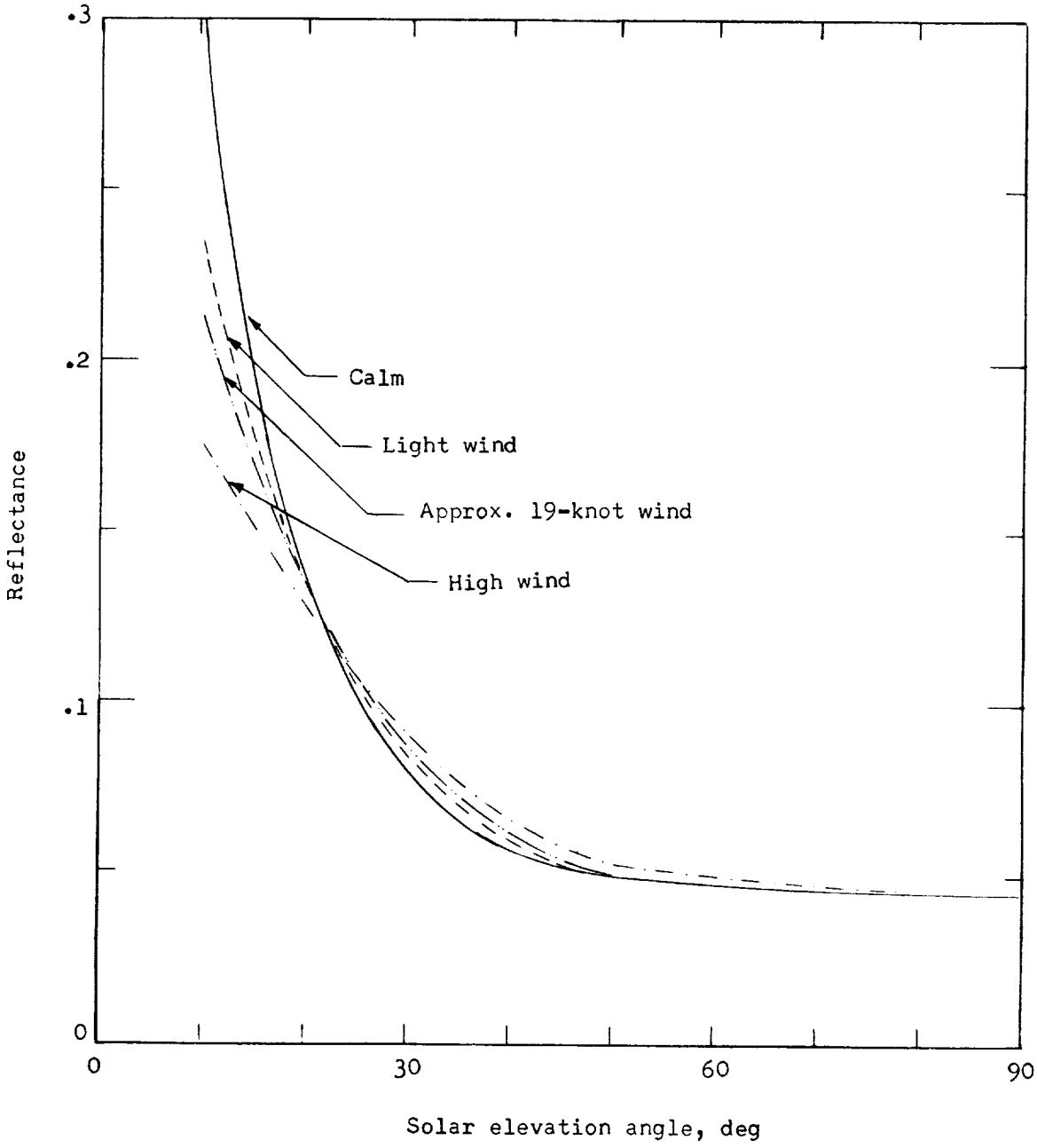

Figure 10.- Theoretical reflectance of smooth water and estimated reflectances (based on Gaussian distribution of surface slopes) of water under high wind and under light wind, as functions of solar elevation angle (from ref. 27).

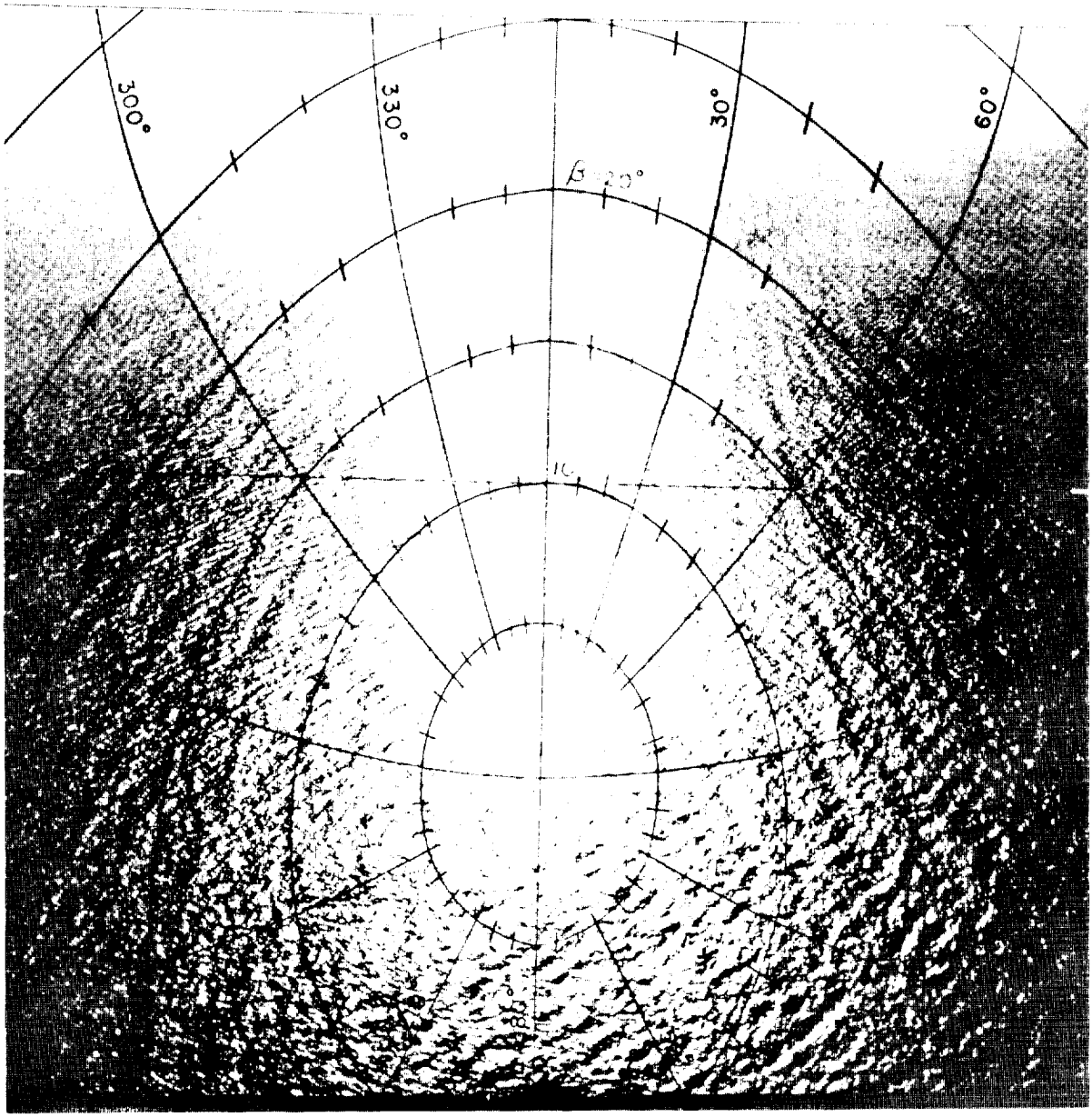

Figure 11.- Photograph of the Pacific Ocean under a 9-knot wind, with the Sun at 50° elevation (from ref. 29). The radial lines are lines of constant azimuth of ascent, and the ovals are lines of constant angle of ascent, of the wave surfaces that reflect sunlight toward the camera.

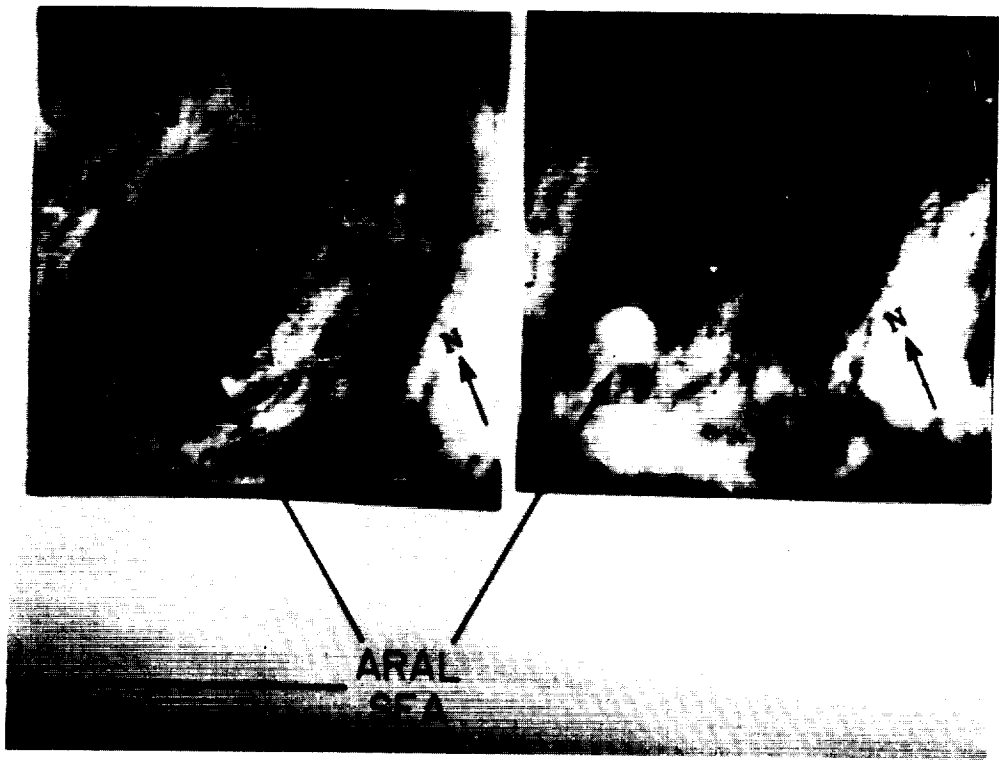

Figure 12.- Two pictures of the Aral Sea, taken about 1 minute apart, by the Tiros I satellite. The picture on the right shows an almost specular reflection of the Sun in the water. Courtesy of David S. Johnson, Meteorological Satellite Laboratory, U.S. Weather Bureau.

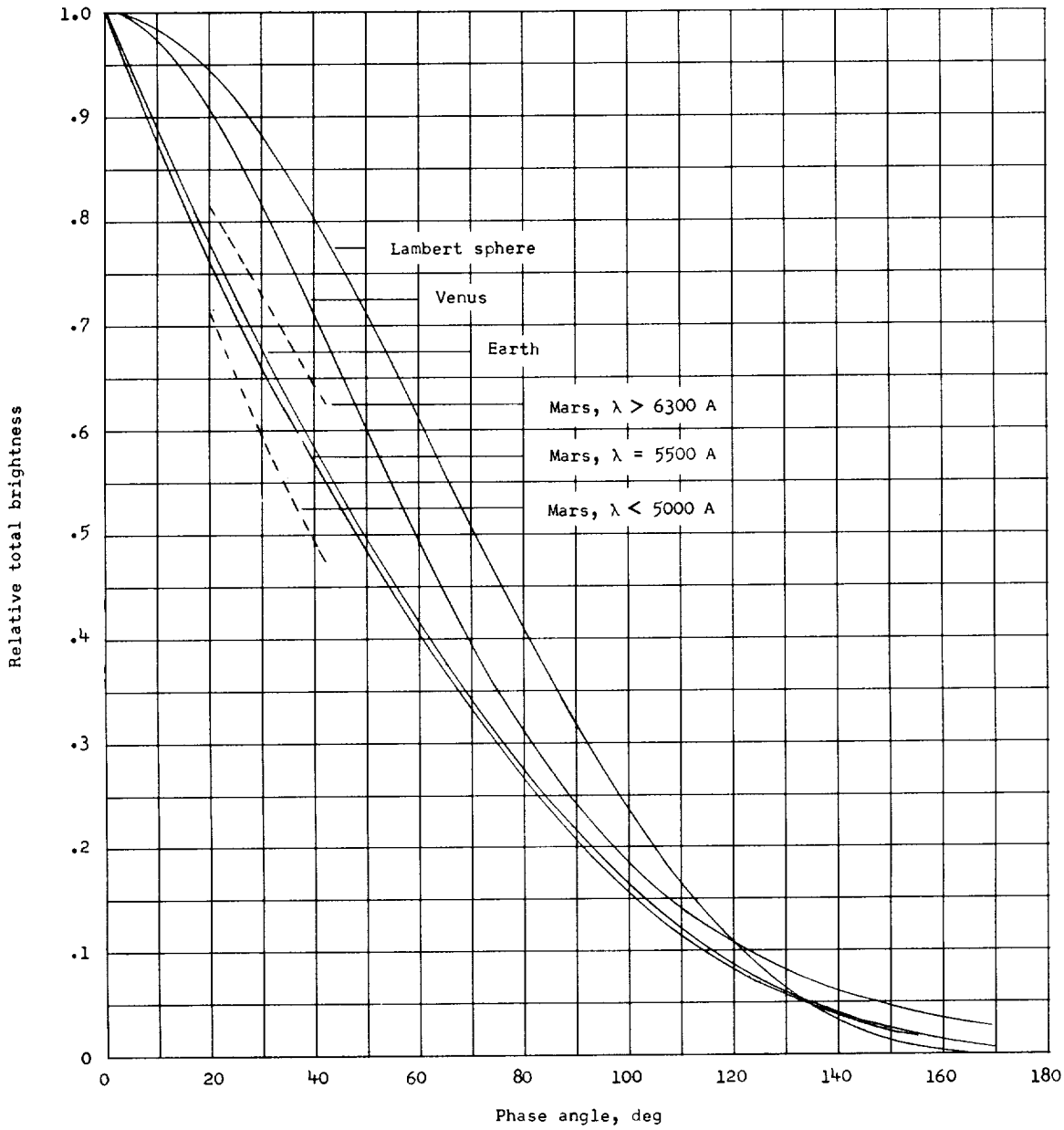

Figure 13.- Angular distribution of reflected radiation (visual) from Earth, Mars, and Venus. Dashed curves indicate the distribution for Mars for the red and the blue regions of the spectrum. Theoretical distribution for a Lambert sphere is shown for comparison (from refs. 33, 59, and 68).

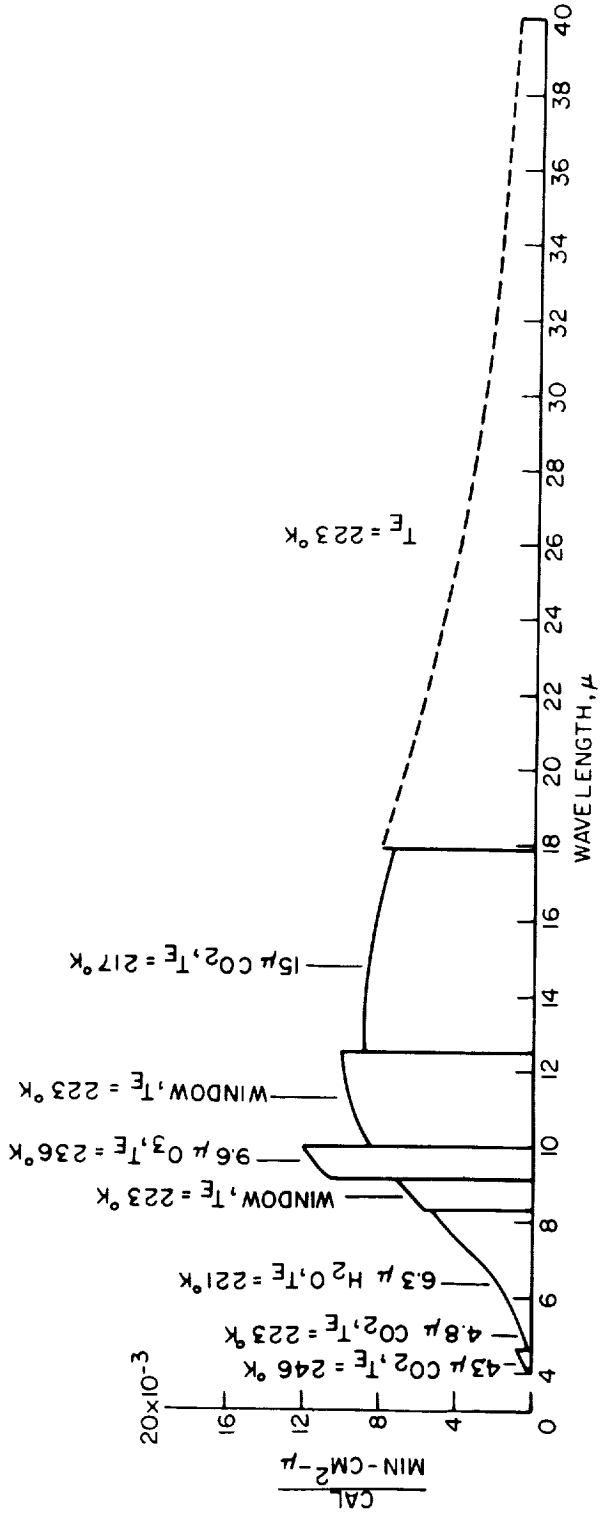

Figure 14.- Estimated spectrum of the vertically outgoing thermal radiation over Norfolk, Va. on March 6, 1960. (T_E is effective thermal radiation temperature.)

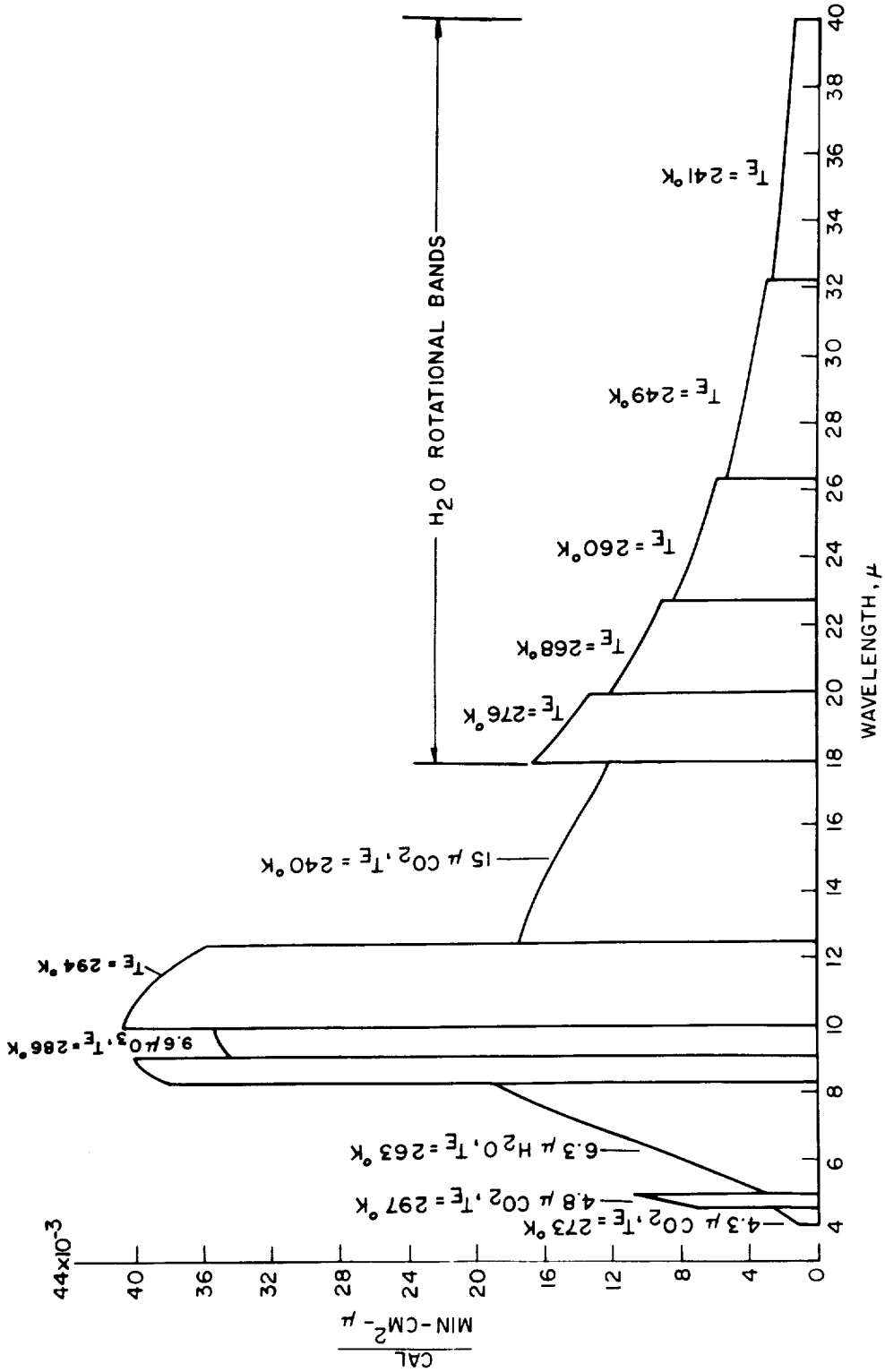

Figure 15.- Estimated spectrum of the vertically outgoing thermal radiation over Miami, Fla. on March 6, 1960. (T_E is effective thermal radiation temperature.)

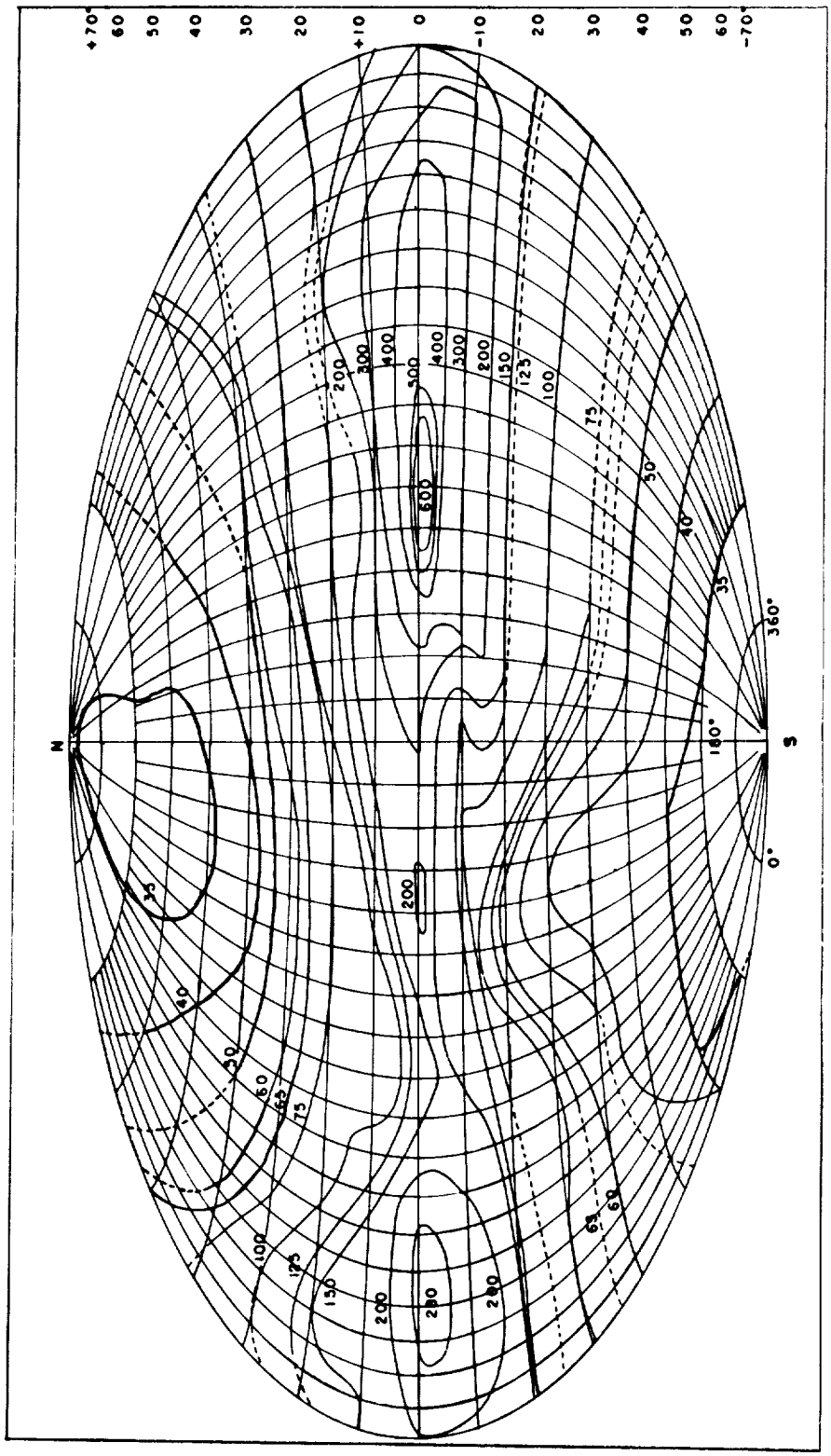

Figure 16.- Contours of brightness of the celestial sphere (shown in galactic coordinates) due to integrated starlight, in tenth-magnitude stars (visual) per square degree (from ref. 40, copyright Jan. 1954 by the University of Chicago).

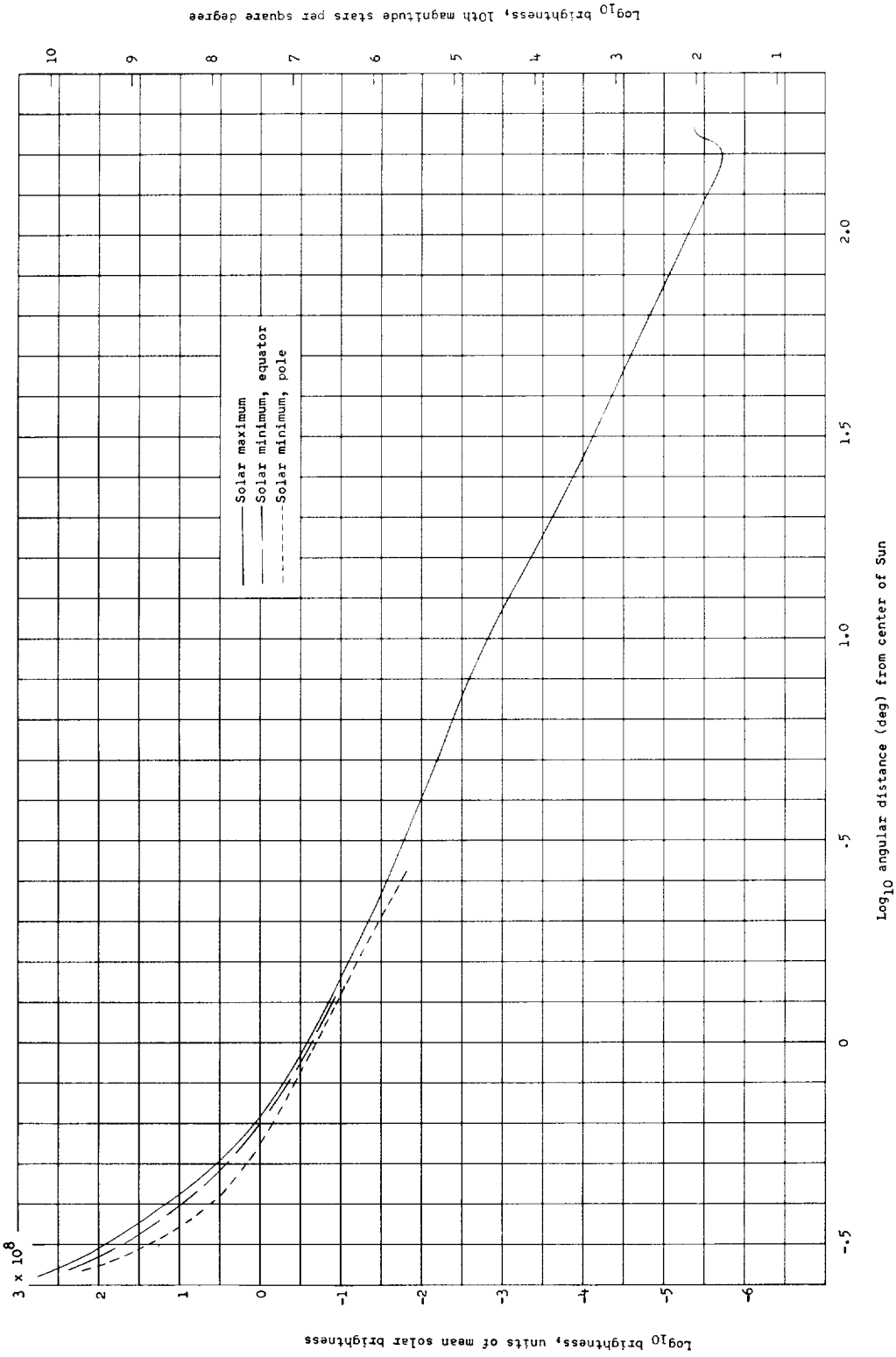

Figure 17.- Brightness of the solar corona and along the center of the zodiacal light (from refs. 13 and 44).

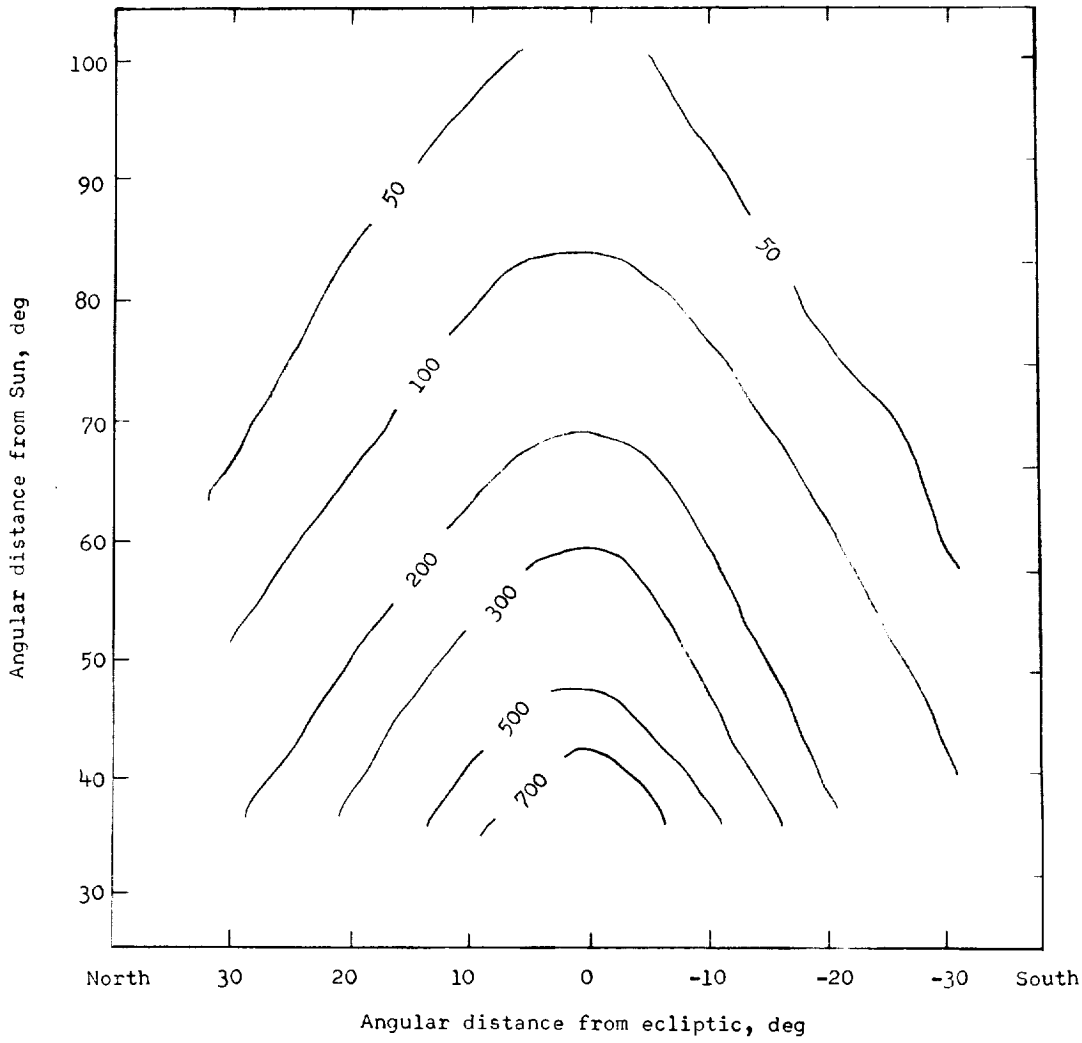

Figure 18.- Contours of intensity of the zodiacal light, measured at 5,410 A (maximum transmission of interference filter), in tenth-magnitude class G2 stars per square degree (from ref. 45).

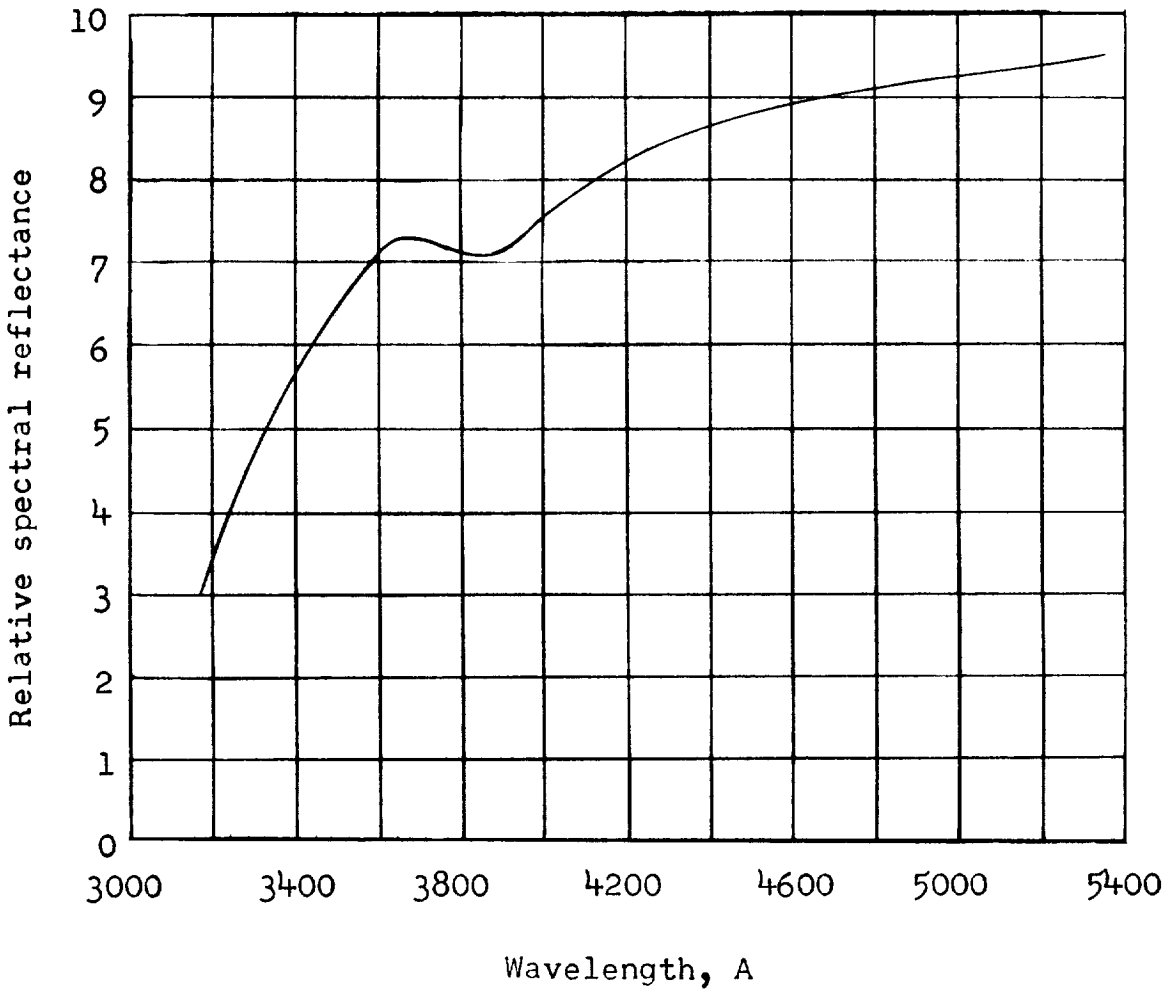

Figure 19.- Relative spectral reflectance of the Moon (from ref. 47).

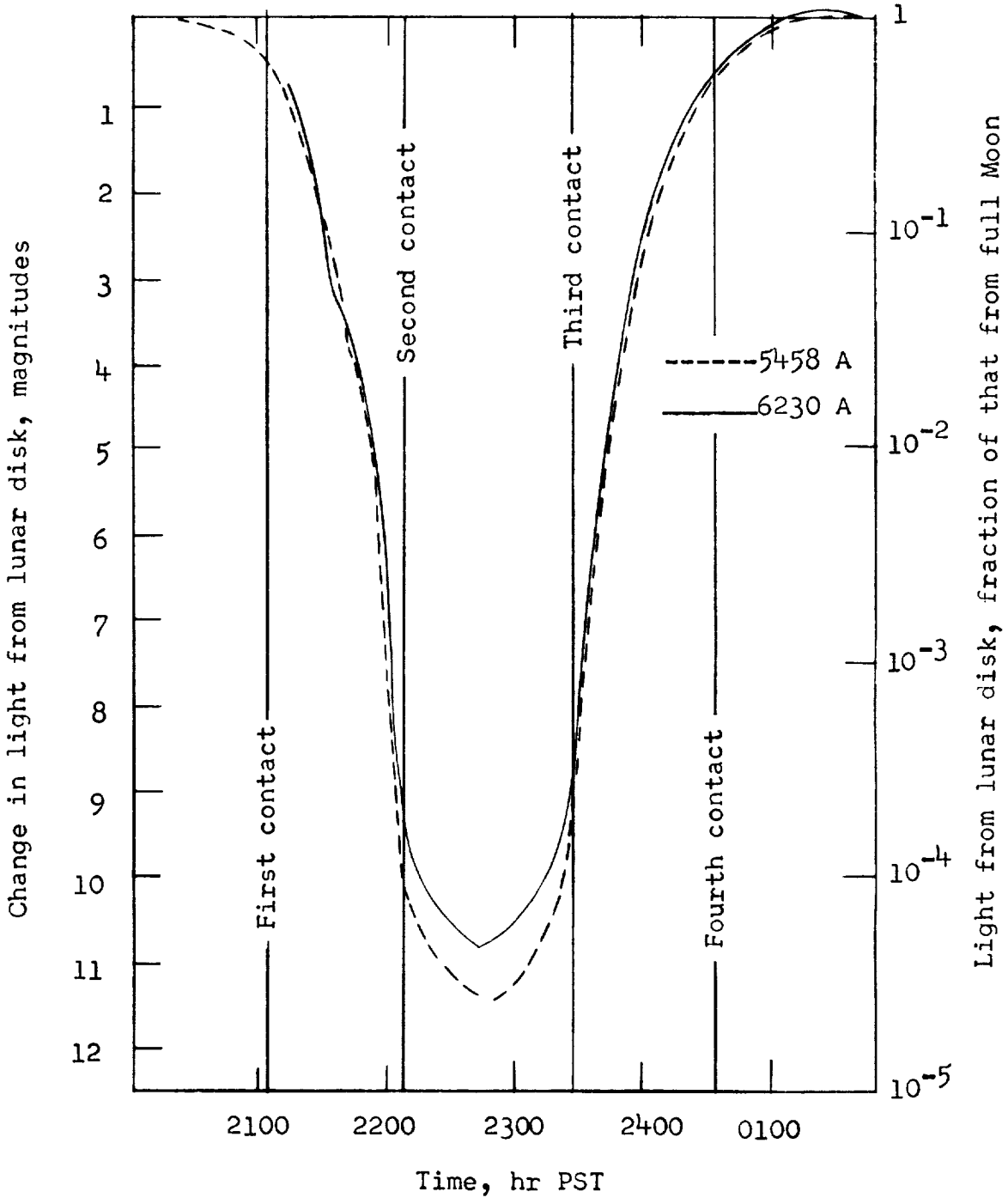

Figure 20.- Variation of average brightness of the Moon during an eclipse, in two wavelengths (from ref. 49).

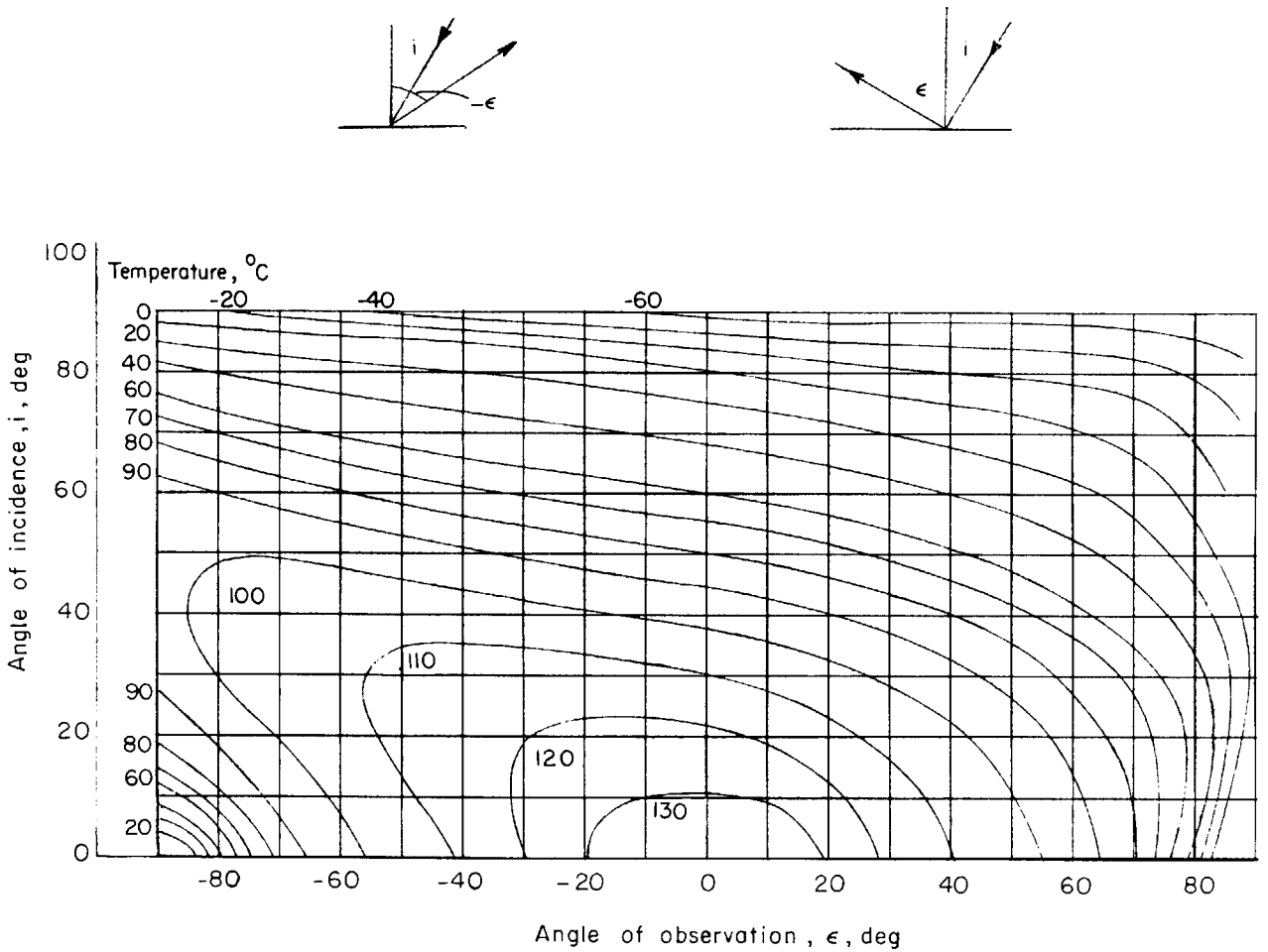

Figure 21.- Effective thermal-radiation temperature, °C, of the sunlit lunar surface, as a function of angle of incidence of the sunlight and angle of observation. Direction of observation is in the plane of incidence of the sunlight.

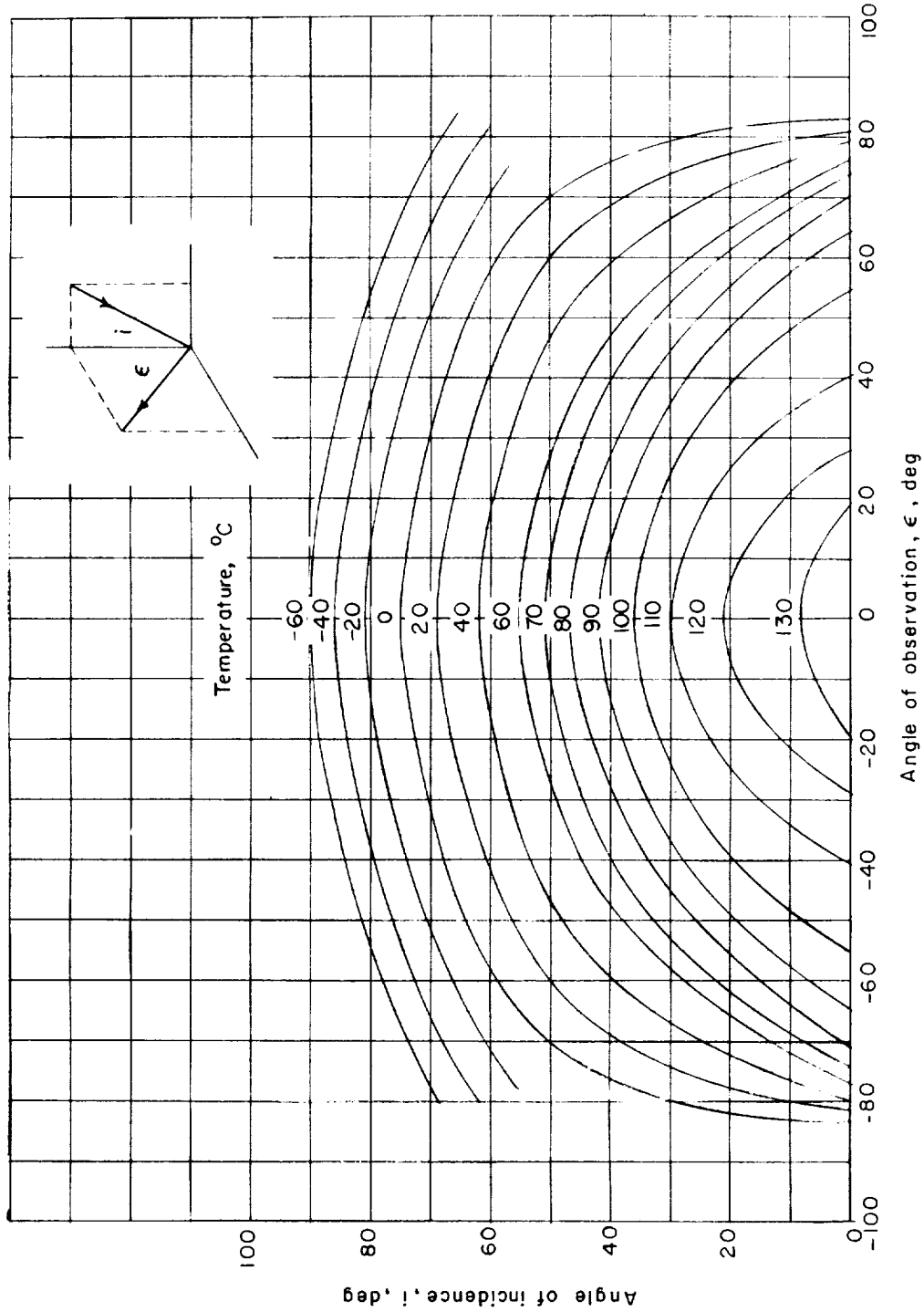

Figure 22.- Effective thermal-radiation temperature, °C, of the sunlit lunar surface, as a function of angle of incidence of the sunlight and angle of observation. The plane of observation is normal to the plane of incidence of the sunlight.

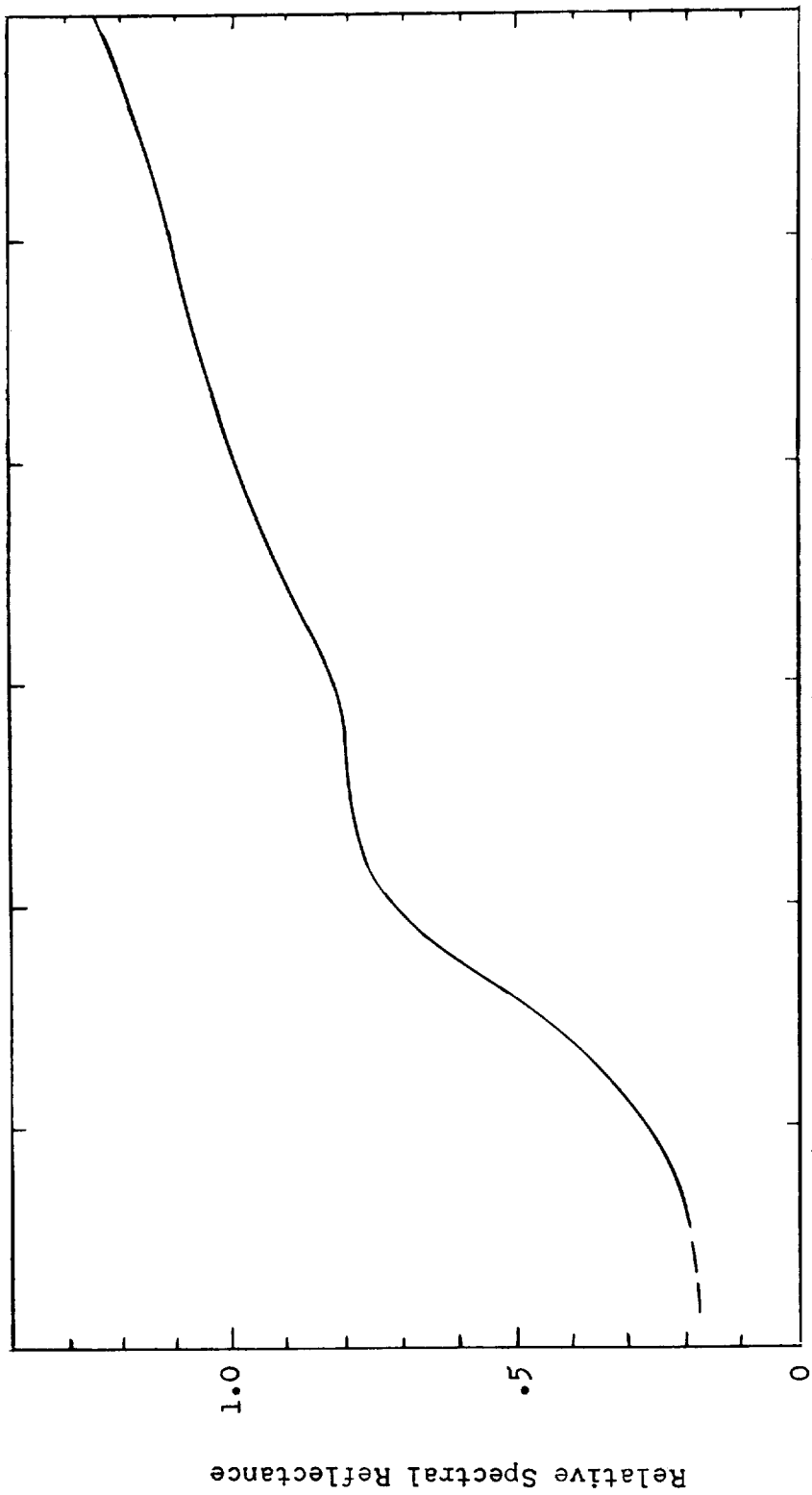

Figure 23.- Relative-spectral-reflectance curve of Venus (from refs. 59 and 60).

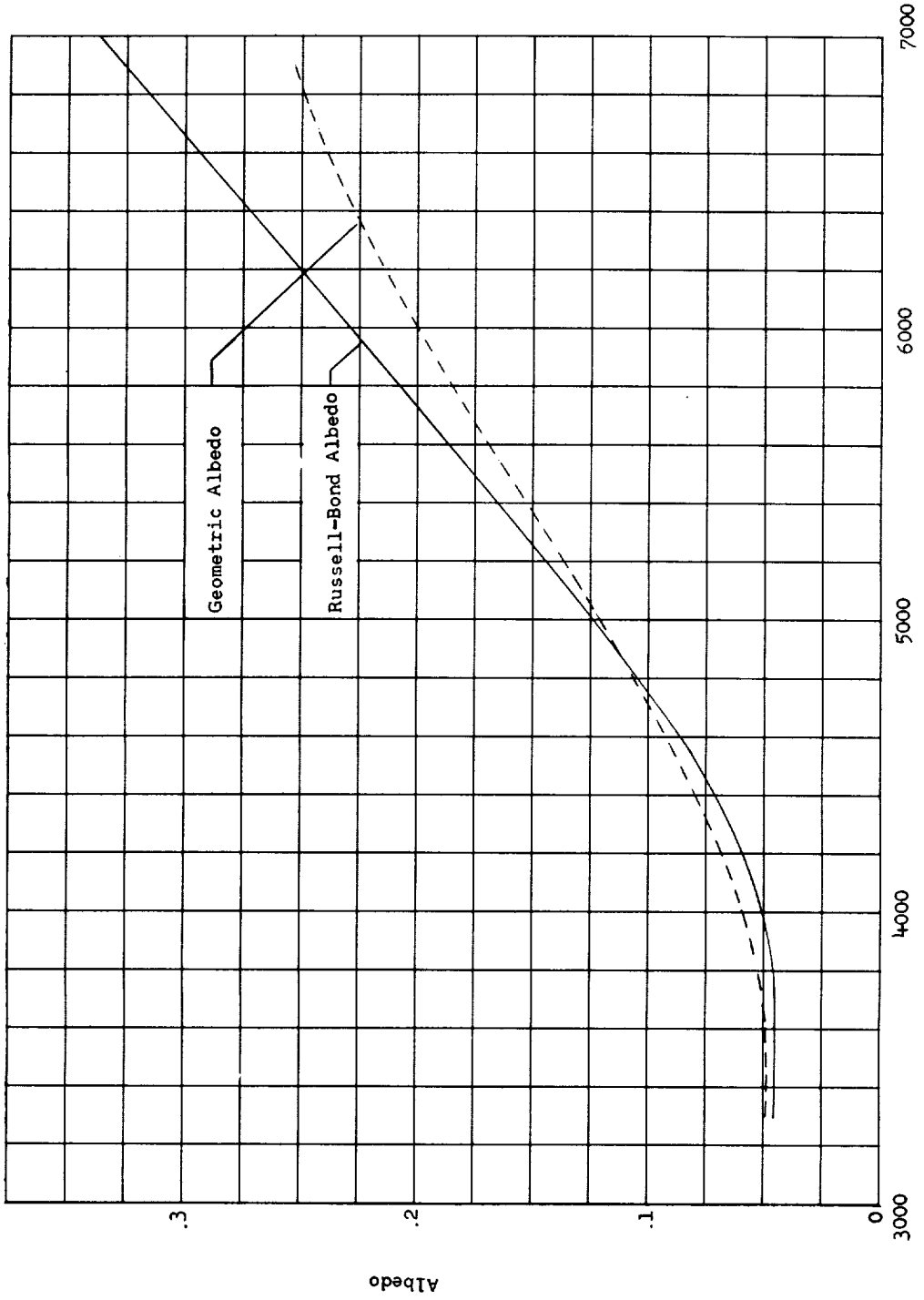

Figure 24.- Spectral albedo curves of Mars (from refs. 59 and 68).

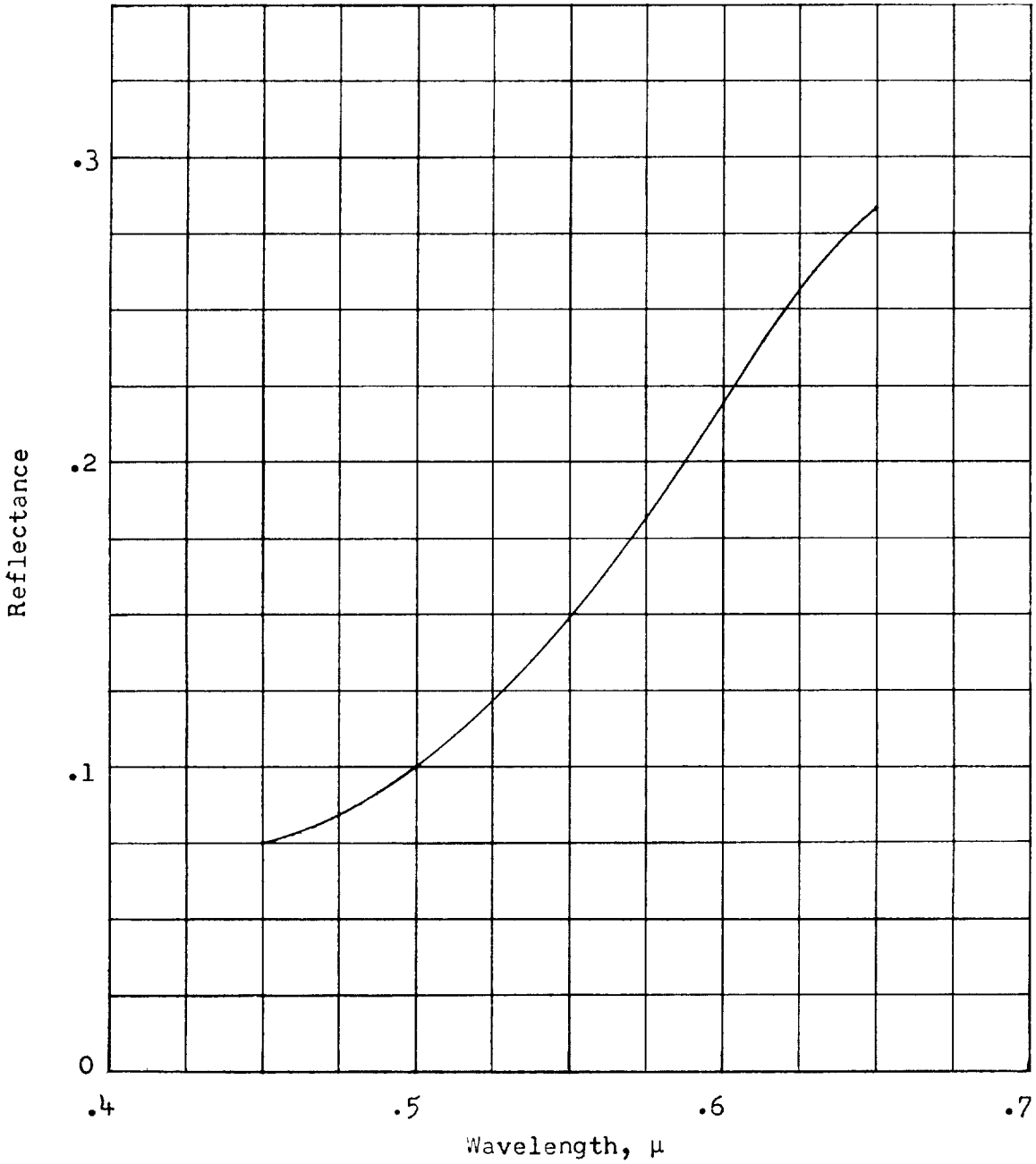

Figure 25.- Spectral reflectance of light areas of Mars, for normal illumination and observation (from ref. 67).

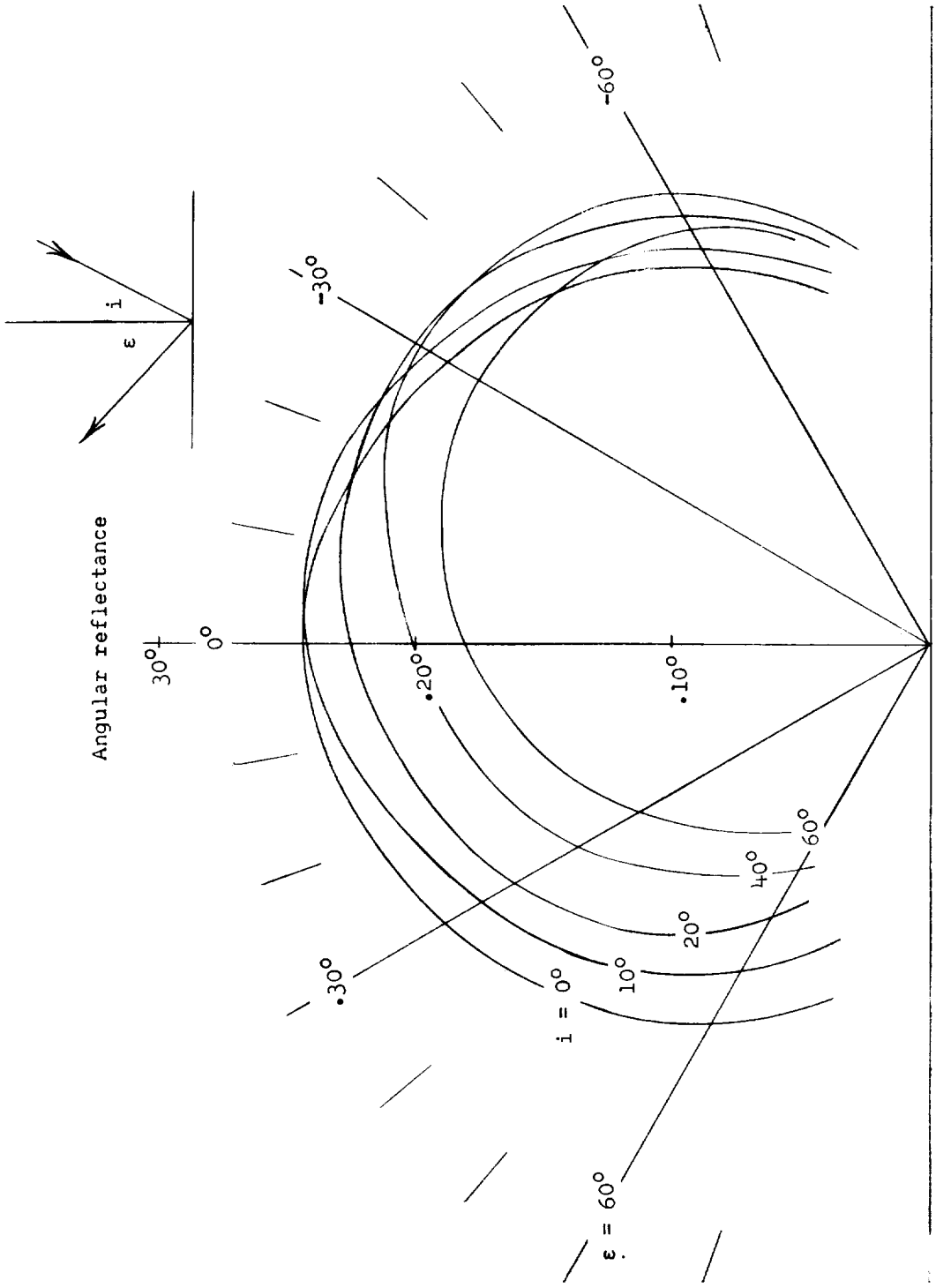

Figure 26.- Angular distribution of reflectance, in the plane of incidence, of the light areas of Mars for $\lambda = 6,200$ A (based on fig. 5 of ref. 67).

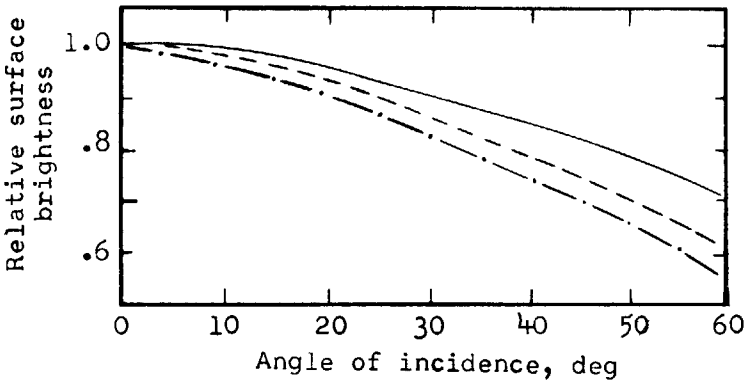

(a) Transparent atmosphere.

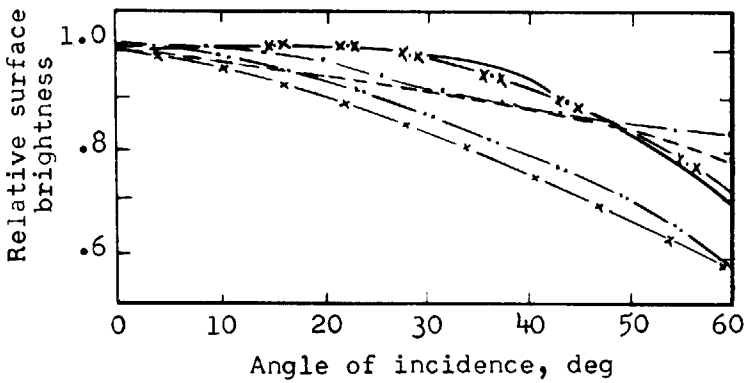

(b) Turbid atmosphere, light area.

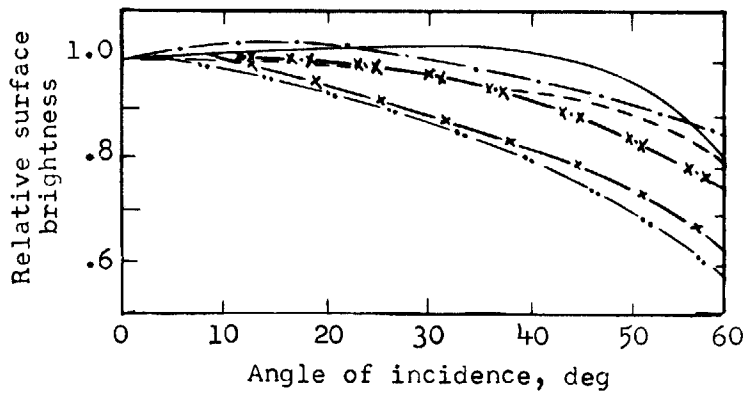

(c) Highly turbid atmosphere, light area.

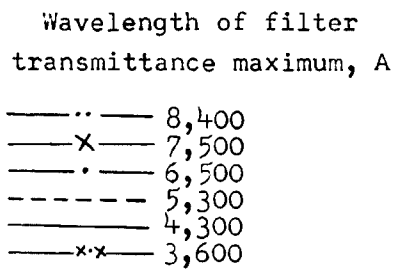

Figure 27.- Distribution of relative surface brightness across the face of Mars in several wavelengths and for three different weather conditions (from ref. 69).

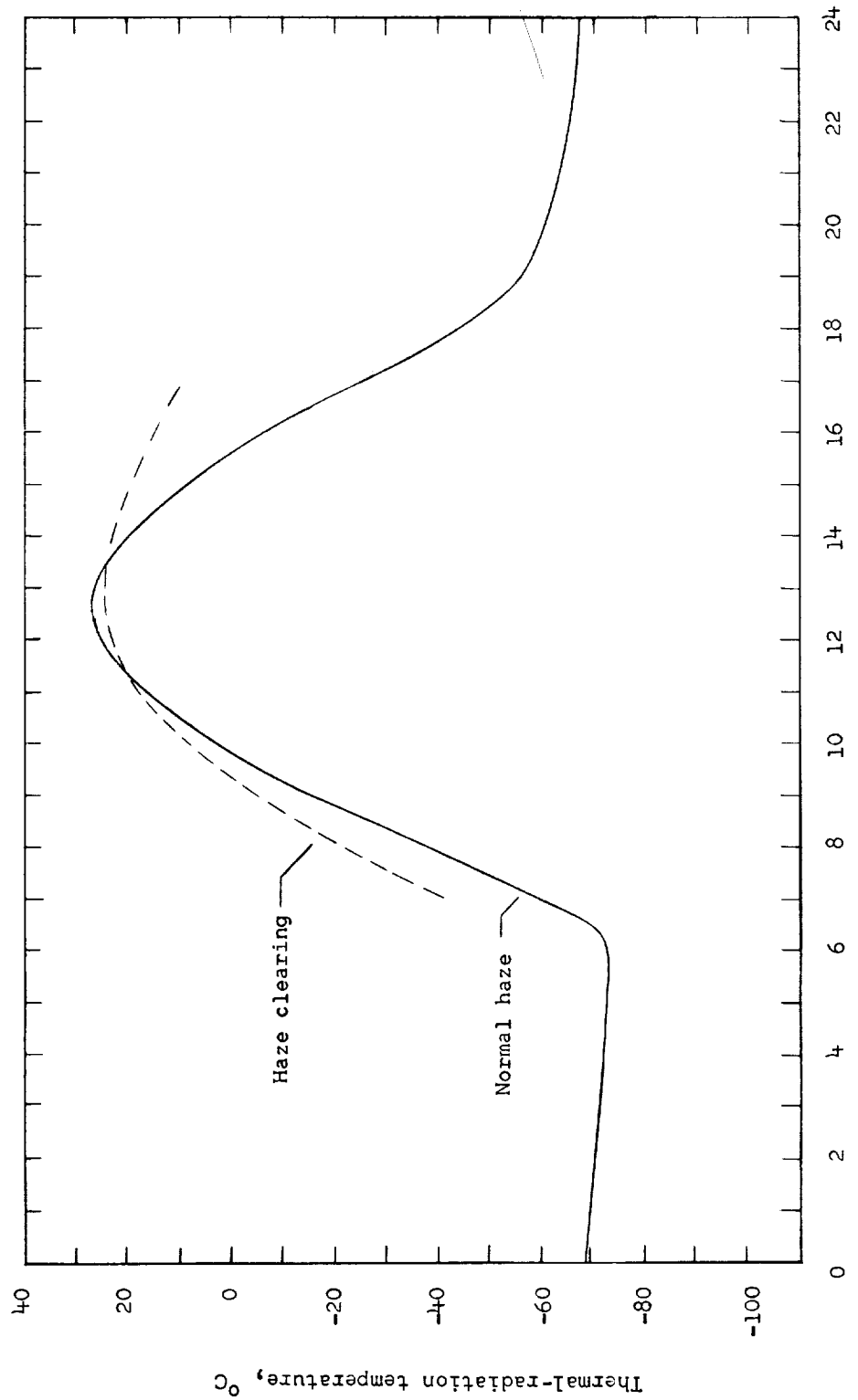

Figure 28.- Thermal-radiation-temperature scan along an east-west line through the center of the Mars disk, about 45° before perihelion (adapted from ref. 62). Late afternoon and night temperatures are extrapolated and estimated. The dashed curve (based on refs. 65 and 70) indicates the modification during a haze clearing.

NASA-Langley, 1962 L-2089